THE ASTROPHYSICAL JOURNAL, 335:74–92, 1988 December 1

IRAS OBSERVATIONS OF AN OPTICALLY SELECTED SAMPLE OF INTERACTING GALAXIES

HOWARD A. BUSHOUSE,[1,2,3] SUSAN A. LAMB,[3,4] AND MICHAEL W. WERNER[1]

Received 1988 March 1; accepted 1988 May 27

ABSTRACT

IRAS observations of a large, morphologically selected sample of strongly interacting disk-type galaxies have demonstrated that galaxy-galaxy collisions can lead to enhanced infrared emission, but not in all cases. Infrared luminosities of the interacting galaxies span a large range, but are about a factor of 2 higher, on average, than those of isolated disk galaxies. The data suggest the existence of a cutoff in blue luminosity, below which no galaxies show markedly enhanced infrared emission. Only the most strongly interacting systems in the sample show extreme values of infrared excess, suggesting that deep, interpenetrating collisions are necessary to drive infrared emission to extreme levels. Comparisons with optical indicators of star formation show that infrared excess and color temperatures correlate with the level of star-formation activity in the interacting galaxies. All interacting galaxies in our sample that exhibit an infrared excess and have higher than normal color temperatures also have optical indicators of high levels of star formation. It is not necessary to invoke processes other than star formation to account for the enhanced infrared luminosity in this sample of interacting galaxies.

Subject headings: galaxies: interactions — galaxies: stellar content — infrared: sources — stars: formation

I. INTRODUCTION

Galaxy collisions and mergers can have dramatic impact upon the morphology and subsequent dynamical evolution of galaxies, as has been shown both from dynamical simulations (e.g., Toomre and Toomre 1972; Miller and Smith 1980) and from comparison of these results with the morphology of actual galaxy pairs and possible merger products. In recent years it has also become apparent that galaxy-galaxy collisions can often lead to enhanced levels of star-formation activity, particularly in the nuclear regions of the interactors (see, e.g., Keel *et al.* 1985; Bushouse 1986*a*), and that interactions may be involved in other forms of enhanced nuclear activity, such as that found in Seyferts and in less energetic low-ionization nuclear emission regions (LINERs) (Stauffer 1981; Goad and Gallagher 1985; Dahari 1985).

Infrared observations have provided further evidence for enhanced star formation in galaxy interactions (e.g., Cutri and McAlary 1985; Joseph *et al.* 1984; Joseph and Wright 1985; Lonsdale, Persson, and Matthews 1984; Rieke *et al.* 1985). The close association between the recently formed stars and the dust and gas from which they formed causes the dust to absorb and reradiate the starlight and assures that much of the luminosity of a group of young stars will emerge in the infrared. The high sensitivity (particularly at long wavelengths) and unbiased nature of the *IRAS* survey make the *IRAS* data base well suited for further studies of this phenomenon.

To date, several analyses of the *IRAS* data have highlighted the effect of interactions on the infrared properties of galaxies. Soifer *et al.* (1984) report in their analysis of the *IRAS* minisurvey data that infrared-selected galaxies have near neighbors 3–5 times as often as expected; this strongly suggests that interacting systems are brighter than normal in the infrared bands sampled by *IRAS*. Lonsdale *et al.* explore this result further, and find that 50%–100% of the minisurvey interacting systems are brighter at 80 μm than at visual wavelengths, as opposed to less than 10% for noninteracting systems. Haynes and Herter (1988) and Kennicutt *et al.* (1987) also find evidence for an enhancement in the far-infrared (FIR) luminosity of binary and interacting galaxies. The criteria for labeling a galaxy "interacting" are not well defined, and various samples may include tidally distorted galaxies and merger products as well as more distant binary encounters. However, it is clear that the environment has a very strong effect on the FIR emission properties of galaxies.

Nevertheless, a close interaction between two galaxies does not inevitably result in a violent burst of star formation. For example, the recent study of 100 pairs of strongly interacting disk galaxies by Bushouse (1986*a*) shows that approximately 30% of the galaxies show only weak or undetectable optical emission lines and have absorption line spectra characteristic of old, elliptical galaxy-like stellar populations. Thus there appears to be a very wide range in the star-formation properties of interacting galaxy systems.

In this paper, we use *IRAS* observations of the Bushouse interacting sample and of about 80 isolated spirals in a further investigation of the enhancements in infrared flux produced by interactions between galaxies. The range of optical and infrared properties displayed by these galaxies allows a comparison of optical and infrared indicators of star formation. Of particular importance is that this is a study of the infrared properties of an optically selected sample of interacting galaxies. It thus bridges the gap between the earlier visual wavelength studies of such optically selected systems and the intensive studies which have shown the prevalence of interacting systems in infrared-selected samples.

In § II we present details of our observed samples of galaxies and a description of our observational and analysis procedures. In § III we present a comparison between the infrared properties of the interacting and isolated galaxy samples. In §§ IV and V we compare classical optical indicators of star formation with the infrared properties of both samples, as well as with various subsamples of the interacting galaxies, each

[1] Space Sciences Division, NASA-Ames Research Center.
[2] NRC/NAS Research Associate.
[3] Guest Investigator, Infrared Processing and Analysis Center.
[4] Departments of Physics and Astronomy, University of Illinois at Urbana-Champaign.

chosen to represent different overall star-formation characteristics.

II. SAMPLE SELECTION AND OBSERVATIONAL PROCEDURES

The sample of interacting galaxies has been taken from Bushouse (1986*b*) and consists of 109 pairs of colliding galaxies, including a few systems that appear to be in the process of merging, selected from the *Uppsala General Catalogue of Galaxies* (Nilson 1973) and the *Atlas of Peculiar Galaxies* (Arp 1966). The galaxies in this sample were chosen on the basis of their optical morphology and include only pairs of galaxies that exhibit features unmistakably associated with strong tidal interactions (e.g., tidal tails and bridges, warped disks, etc.). Membership in this sample has also been limited to systems in which at least one of the galaxies shows some evidence of a stellar disk. Approximately 80% of the systems are spiral-spiral pairs of comparable brightness, 10% are spiral-elliptical pairs, and the remaining 10% are spirals with a smaller companion or merging systems. These interacting systems were chosen without regard to any previous knowledge of such parameters as optical colors, spectral characteristics, group or cluster membership, or level of infrared or radio emission. As a result, this sample of interacting galaxies is fundamentally different from *IRAS*-selected samples of galaxies which have been studied previously and which may be biased toward starburst galaxies and galaxies with active nuclei (e.g., Allen, Roche, and Norris 1985; Elston, Cornell, and Lebofsky 1985; Houck *et al.* 1985; Sanders *et al.* 1988).

Of the 109 interacting systems in the original sample, three were not observed by *IRAS* and an additional 24 systems have IR fluxes that are too low to be included in the Point Source Catalog. These latter 24 undetected systems were examined using the ADDSCAN utility at the IPAC and all but three were subsequently detected in at least one of the *IRAS* bands. Thus we have a sample of 106 interacting systems, three of which (Arp 100, UGC 1228, and UGC 7891) have only upper limits to their fluxes in all four *IRAS* bands.

Our comparison sample of galaxies is composed of 83 isolated galaxies, type Sa through Im, chosen from the list of Kennicutt and Kent (1983). Their original list is essentially a magnitude-limited sample of galaxies, mostly spirals, chosen from the *Revised Shapley-Ames Catalogue of Bright Galaxies* (Sandage and Tammann 1981; hereafter RSA). Only galaxies with optical diameters less than 4′ have been included in our sample, so the total IR fluxes are reasonably well estimated by the *IRAS* point-source extraction procedure. This is not a problem for the interacting galaxies since they are more distant, on average, than the isolated galaxies and generally have angular diameters less than 90″. Elliptical and S0-type galaxies have been left out of the comparison sample to allow meaningful comparisons with the predominantly disk-type systems contained in the sample of interacting galaxies. The Seyfert galaxies NGC 1068 and NGC 6814 have also been omitted from the sample of isolated spirals because we are primarily interested in the characteristics of galaxies experiencing "normal" star formation activity and also because of the rarity of Seyferts in the sample of interacting galaxies used here (Bushouse 1986*a*). We have also eliminated all galaxies (as indicated by Kennicutt and Kent) that are probable Virgo members since they are not truly isolated.

Observed optical and *IRAS* data for the samples of interacting and isolated galaxies are presented in Tables 1 and 2, respectively. Data for the interacting galaxies are from the following sources. Radial velocities are taken from Bushouse (1986*b*) and are from either H I 21 cm observations or optical spectral line measurements. Total apparent blue magnitudes are from the *Second Reference Catalogue of Bright Galaxies* (de Vaucouleurs, de Vaucouleurs, and Corwin 1976) when available, or from UGC listings of m_b which have been transformed onto the B_T system according to the procedures outlined in Fisher and Tully (1981). Global Hα emission-line fluxes are available for about 40 of the interacting systems from Bushouse (1987). *IRAS* data for 94 of the pairs come from measurements made using the ADDSCAN utility at the IPAC, while data for the remaining systems are from *Catalogued Galaxies and Quasars Observed in the IRAS Survey* (1985; hereafter the Extragalactic Catalog). Upper limits to the fluxes for objects not detected using ADDSCAN are 3 σ levels of the rms noise in each wavelength band. A complete cross-reference of Arp Atlas, NGC, and UGC designations for the interacting systems can be found in Bushouse (1986*b*).

For the isolated galaxies, radial velocities are from either H I 21 cm observations (Fisher and Tully 1981; Bottinelli, Gouguenheim, and Paturel 1982; Huchtmeier 1982) or the RSA, and apparent *B* magnitudes are from either the RSA or Keel (1983). Global Hα emission line fluxes and equivalent widths have been recalculated from the data of Kennicutt (1983) so that they are on the same scale as the data for the interacting galaxies. Following Kennicutt's suggestion, we have corrected their observed Hα + [N II] emission-line fluxes and equivalent widths by a factor of 0.75 to account, in an average way, for contributions from the [N II] λ6548 + 6583 emission. The Hα data for the interacting galaxies have been corrected in a similar fashion. We use *IRAS* data from the Extragalactic Catalog for the entire sample of isolated galaxies. Approximately 50% of the isolated galaxies detected at 60 and 100 μm are undetected in either the 12 or 25 μm bands, or both.

Distances for galaxies in both samples have been calculated from their radial velocities assuming $H_0 = 75$ km s^{-1} Mpc^{-1}. No attempt has been made to correct any of the optical data for the effects of extinction internal to the galaxies. Corrections have been made for Galactic extinction only, using values of A_B from Burstein and Heiles (1982, 1984).

Derived luminosities, luminosity ratios, and colors for the interacting and isolated galaxies are also presented in Tables 1 and 2. Here L_{IR} is the FIR luminosity calculated according to the procedure outlined in Appendix B of the Extragalactic Catalog. This value represents the total flux in an 80 μm wide square bandpass centered at 82 μm and is essentially independent of the intrinsic energy distribution for typical galaxies. A comparison of the median[5] values of various observed and derived parameters for the two samples is given in Table 3.

A major shortcoming of the *IRAS* data for the interacting systems is that the individual galaxies within most pairs are not resolved, due to their small angular separations. Therefore observed *IRAS* fluxes refer to the total for each pair, with no additional information as to how the flux is distributed between the galaxies. The optical Hα data, on the other hand, are available on a per-galaxy basis, while the blue magnitudes are a mixture of measurements per galaxy and per pair. In an

[5] We most often use the median values of distributions, as opposed to the mean, since the distributions of most observed parameters are asymmetric (usually due to the presence of a high-end tail) and the mean value is then biased by a few extreme values. An exception to this is where we deal with small samples of objects (e.g., § V), because in these situations the median can be misleading due to statistical noise. In these cases we use the mean value.

TABLE 1

INTERACTING GALAXIES

Name	V_0	B_T	log F(Hα)	$f_\nu(12)$	$f_\nu(25)$	$f_\nu(60)$	$f_\nu(100)$	$\log \frac{f(12)}{f(25)}$	log F(IR)	L_B	L_{IR}/L_B	$L_{H\alpha}/L_B$
	D	A_B	W_λ(Hα)	σ	σ	σ	σ	$\log \frac{f(60)}{f(100)}$	log $L_{H\alpha}$	L_{IR}	$L_{IR}/L_{H\alpha}$	$L_{H\alpha}$/area
(1)	(2)	(3)	(4)	(5)	(6)	(7)	(8)	(9)	(10)	(11)	(12)	(13)
A256	8253	...	-12.17	0.29	1.33	6.70	11.13	-0.66	-9.45	...	...	...
	110.0	0.01	44	35	57	40	53	-0.22	41.99	134.06	527	7.59
U248	10391	14.62	...	<0.13	< 0.14	0.35	0.75	...	-10.68	5.89	2.1	...
	138.5	0.06	...	42	45	57	150	-0.33	...	12.51	...	...
A100	6157	15.00	...	<0.12	< 0.16	< 0.10	< 0.25	...	<-11.19	1.38	< 1.0	...
	82.1	0.01	...	41	54	32	84	...	...	< 1.34	...	...
U480	11358	13.57	-12.78	<0.13	< 0.09	1.40	4.42	...	-9.99	20.42	3.6	0.006
	151.4	0.17	6	44	30	28	103	-0.50	41.70	71.99	556	1.02
A251	22906	...	...	<0.25	< 0.25	0.72	1.31	...	-10.40	...	...	...
	305.4	0.00	...	...	...	...	...	-0.26	...	116.76	...	...
U593/4	5559	13.70	-12.61	0.23	1.15	8.48	15.78	-0.70	-9.32	5.37	15.1	0.010
	74.1	0.41	8	18	22	27	102	-0.27	41.30	80.78	1546	5.89
U603	13932	15.11	...	<0.10	< 0.14	0.24	1.31	...	-10.61	7.41	3.6	...
	185.8	0.16	...	34	47	47	152	-0.74	...	26.14	...	...
U717/9	11481	13.62	...	0.13	< 0.17	0.46	1.55	>-0.12	-10.46	18.62	1.4	...
	153.1	0.09	...	37	56	63	287	-0.53	...	25.54	...	...
U813/6	5466	13.80	-12.28	0.28	0.34	2.76	7.58	-0.08	-9.73	5.13	6.0	0.022
	72.9	0.49	25	27	26	36	90	-0.44	41.64	30.71	270	6.17
U966	2272	12.05	...	0.84	3.09	31.07	51.67	-0.57	-8.78	2.95	16.2	...
	30.3	0.05	...	50	42	52	100	-0.22	...	47.57	...	...
U993	2999	15.19	...	<0.11	< 0.20	0.17	< 0.31	...	<-11.03	0.31	< 1.5	...
	40.0	0.14	...	35	67	48	104	>-0.26	...	< 0.48	...	...
U1063/5	5929	14.10	-12.70	0.20	0.40	1.15	3.49	-0.30	-10.09	3.55	4.5	0.012
	79.1	0.21	18	43	58	41	192	-0.48	41.22	15.75	364	2.04
U1228	4133	14.78	-13.18	<0.11	< 0.12	< 0.10	< 0.57	...	<-10.98	0.93	< 1.1	0.008
	55.1	0.23	...	35	40	34	191	...	40.43	< 0.99	< 139	1.62
U1720	9264	14.21	-12.32	0.29	0.64	5.26	9.59	-0.34	-9.53	7.08	19.6	0.034
	123.5	0.11	45	58	62	37	125	-0.26	41.97	140.38	574	53.70
U1818	...	15.91	...	<0.60	< 0.46	0.61	< 1.61	...	<-10.40	...	...	...
	...	0.00	...	...	...	...	...	>-0.42	...	...	...	...
U2320	10471	14.86	-13.87	<0.12	< 0.17	0.15	< 0.78	...	<-10.83	6.31	< 1.4	0.002
	139.6	0.36	2	41	57	47	260	>-0.72	40.58	< 9.06	< 896	0.50
U2388/9	8490	13.59	...	0.33	0.71	5.23	11.21	-0.33	-9.51	11.22	11.1	...
	113.2	0.18	...	...	...	...	...	-0.33	...	125.11	...	...
U2992	4984	15.00	...	0.10	0.21	1.03	1.33	-0.32	-10.30	1.38	5.0	...
	66.5	0.48	...	22	34	27	81	-0.11	...	6.88	...	...
U3031/2	4645	13.57	...	<0.09	< 0.10	0.35	0.93	...	-10.64	3.63	0.8	...
	61.9	0.25	...	30	32	31	86	-0.42	...	2.80	...	...
N1614	4636	13.60	...	1.60	7.87	32.43	39.00	-0.69	-8.81	3.47	53.6	...
	61.8	0.22	...	43	31	99	380	-0.08	...	185.05	...	...
U3706	6299	14.46	...	<0.07	0.07	0.39	0.83	< 0.00	-10.64	3.09	1.6	...
	84.0	0.30	...	22	20	38	86	-0.33	...	5.10	...	...
U3737	4384	14.94	...	<0.10	< 0.15	0.45	1.18	...	-10.53	0.98	3.2	...
	58.5	0.32	...	32	49	35	112	-0.42	...	3.14	...	...
A250	24182	...	...	<0.13	< 0.14	0.15	0.59	...	-10.91	...	...	...
	322.4	0.17	...	44	47	34	140	-0.59	...	40.49	...	...
U4264	4019	12.88	...	0.13	0.33	2.30	7.21	-0.40	-9.78	4.68	3.2	...
	53.6	0.14	...	40	48	29	129	-0.50	...	15.04	...	...
U4509	5453	14.40	...	0.32	1.85	23.97	29.18	-0.76	-8.94	2.04	93.7	...
	72.7	0.09	...	23	74	53	96	-0.09	...	189.37	...	...
U4653	16182	14.70	...	0.10	0.24	2.16	5.49	-0.38	-9.86	13.18	15.4	...
	215.8	0.06	...	20	53	33	103	-0.41	...	202.91	...	...
U4718	3102	14.10	...	<0.13	0.12	1.88	3.03	< 0.03	-10.00	0.85	6.2	...
	41.4	0.08	...	42	37	29	107	-0.21	...	5.34	...	...
U4744	2350	14.05	...	<0.10	< 0.18	1.06	3.52	...	-10.10	0.52	4.6	...
	31.3	0.10	...	34	60	21	103	-0.52	...	2.44	...	...
U4757	3309	13.80	-12.78	<0.08	0.44	1.45	2.59	<-0.74	-10.10	1.29	3.8	0.008
	44.1	0.08	21	28	77	39	63	-0.25	40.61	4.87	460	23.44
U4881	11912	14.62	...	0.20	0.69	6.18	10.78	-0.54	-9.47	7.24	36.6	...
	158.8	0.00	...	42	36	50	62	-0.24	...	267.49	...	...
A252	9434	...	...	<0.26	0.99	3.88	4.03	<-0.58	-9.75	...	...	...
	125.8	0.28	...	...	...	...	...	-0.02	...	86.56	...	...
U5265/9	1678	12.59	...	0.15	0.31	2.34	5.80	-0.32	-9.83	1.10	2.1	...
	22.4	0.17	...	27	30	25	243	-0.39	...	2.33	...	...
U5304	11991	14.54	-12.70	<0.07	< 0.21	0.85	1.67	...	-10.31	8.13	4.7	0.020
	159.9	0.04	...	24	71	36	109	-0.29	41.79	38.66	239	3.63

TABLE 1—*Continued*

Name	V_0	B_T	log F(Hα)	$f_\nu(12)$	$f_\nu(25)$	$f_\nu(60)$	$f_\nu(100)$	log $\frac{f(12)}{f(25)}$	log F(IR)	L_B	L_{IR}/L_B	$L_{H\alpha}/L_B$
	D	A_B	W_λ(Hα)	σ	σ	σ	σ	log $\frac{f(60)}{f(100)}$	log $L_{H\alpha}$	L_{IR}	$L_{IR}/L_{H\alpha}$	$L_{H\alpha}$/area
(1)	(2)	(3)	(4)	(5)	(6)	(7)	(8)	(9)	(10)	(11)	(12)	(13)
U5367	7048	15.19	...	<0.10	< 0.09	0.13	0.45	...	-11.00	1.51	1.8	...
	94.0	0.01	...	32	31	36	120	-0.54	...	2.74	...	...
U5600/9	2946	13.50	-12.03	0.23	0.67	3.63	5.90	-0.46	-9.72	1.26	7.4	0.036
	39.3	0.01	...	26	24	43	75	-0.21	41.24	9.27	205	12.59
U5617/20	1123	11.85	...	0.67	1.75	7.84	16.93	-0.42	-9.33	0.85	3.9	...
	15.0	0.02	...	...	...	...	...	-0.33	...	3.29	...	...
U5643	9899	14.10	...	0.10	0.20	1.27	3.34	-0.30	-10.08	8.13	5.6	...
	132.0	0.00	...	28	25	28	111	-0.42	...	45.43	...	...
U5773	6132	13.54	...	<0.14	< 0.17	0.24	0.80	...	-10.75	5.37	0.7	...
	81.8	0.04	...	46	55	36	105	-0.52	...	3.78	...	...
U5931/5	1620	11.74	...	<0.25	0.62	8.01	16.25	<-0.39	-9.33	1.91	3.5	...
	21.6	0.01	...	...	...	...	...	-0.31	...	6.72	...	...
U5938/42	10684	14.94	...	0.09	0.11	0.67	2.34	-0.09	-10.29	4.47	7.2	...
	142.5	0.04	...	22	19	28	95	-0.54	...	32.91	...	...
U5984	10402	14.38	...	<0.10	< 0.15	0.19	1.02	...	-10.72	7.08	1.6	...
	138.7	0.03	...	34	51	42	78	-0.73	...	11.41	...	...
U6224	8687	14.46	...	<0.12	0.63	4.06	8.17	<-0.72	-9.63	4.47	22.0	...
	115.8	0.00	...	40	37	45	79	-0.30	...	99.38	...	...
U6471/2	3255	11.87	...	4.04	25.18	113.76	129.37	-0.79	-8.27	6.76	46.0	...
	43.4	0.00	...	28	38	59	143	-0.06	...	314.27	...	...
U6527	7930	14.46	-13.25	0.17	0.30	0.74	2.34	-0.25	-10.27	3.72	5.0	0.005
	105.7	0.00	8	26	41	32	103	-0.50	40.88	18.94	952	7.59
U6643	7001	13.97	...	<0.17	0.28	2.83	6.73	<-0.22	-9.75	4.57	10.5	...
	93.3	0.01	...	58	44	51	112	-0.38	...	48.67	...	...
A248	5097	...	-12.34	<0.12	0.60	2.59	5.41	<-0.70	-9.82	...	...	...
	68.0	0.00	55	39	50	43	169	-0.32	41.40	22.25	333	60.26
U6865	5933	14.46	...	0.19	0.26	2.34	6.61	-0.14	-9.80	2.09	14.9	...
	79.1	0.00	...	29	30	38	146	-0.45	...	31.43	...	...
N4038/9	1439	11.30	-10.99	1.41	4.80	38.84	83.75	-0.53	-8.63	2.34	11.3	0.051
	19.2	0.05	...	56	37	76	128	-0.33	41.67	26.75	220	25.12
U7070	2663	15.02	...	<0.08	< 0.08	0.19	0.64	...	-10.85	0.25	2.2	...
	35.5	0.00	...	25	27	27	82	-0.53	...	0.56	...	...
U7085A	6976	14.78	-13.03	<0.12	0.31	1.89	2.74	<-0.41	-10.02	2.14	12.1	0.012
	93.0	0.00	...	39	23	32	115	-0.16	40.98	26.14	1028	21.38
U7230	7042	14.54	...	<0.10	< 0.12	0.48	1.01	...	-10.55	3.02	2.6	...
	93.9	0.10	...	32	39	36	72	-0.32	...	7.89	...	...
U7277	6674	14.21	...	<0.12	< 0.15	0.78	1.62	...	-10.34	3.31	3.4	...
	89.0	0.00	...	40	51	41	118	-0.32	...	11.41	...	...
U7575	697	11.70	...	<0.26	< 0.75	2.04	3.99	...	-9.93	0.41	0.8	...
	9.3	0.12	...	...	...	...	...	-0.29	...	0.31	...	...
U7776	2186	12.10	...	1.03	1.52	16.65	59.32	-0.17	-8.89	2.51	13.7	...
	29.1	0.00	...	41	55	61	197	-0.55	...	34.46	...	...
U7891	7046	15.11	...	<0.10	< 0.18	< 0.05	< 0.28	...	<-11.29	1.70	< 0.8	...
	93.9	0.06	...	32	60	16	93	...	...	< 1.44	...	...
U7905	5053	13.97	...	<0.10	0.18	1.89	3.26	<-0.26	-9.99	2.40	6.0	...
	67.4	0.02	...	34	28	56	280	-0.24	...	14.70	...	...
U7910	3623	15.02	...	<0.08	< 0.08	0.35	0.99	...	-10.62	0.47	3.7	...
	48.3	0.00	...	26	28	36	72	-0.45	...	1.73	...	...
U7936	7450	14.86	...	<0.14	< 0.10	0.54	0.97	...	-10.53	2.29	4.0	...
	99.3	0.00	...	46	33	56	77	-0.25	...	9.27	...	...
U7938/9	6608	13.97	-12.92	0.14	0.45	2.76	5.41	-0.51	-9.80	4.07	9.3	0.007
	88.1	0.01	15	22	30	31	112	-0.29	41.05	38.66	1306	16.22
U8034	789	14.62	...	<0.10	< 0.15	0.67	1.47	...	-10.39	0.03	4.2	...
	10.5	0.05	...	35	49	60	138	-0.34	...	0.14	...	...
U8135	7122	14.05	...	0.35	1.47	6.17	8.23	-0.62	-9.52	4.47	19.4	...
	95.0	0.01	...	27	34	33	134	-0.13	...	86.56	...	...
U8315	1208	15.19	...	<0.12	< 0.08	0.18	< 0.31	...	<-11.01	0.04	< 1.8	...
	16.1	0.00	...	40	26	31	103	>-0.24	...	< 0.08	...	...
U8335	9252	14.21	-12.29	0.37	2.07	11.41	14.13	-0.75	-9.26	6.61	39.8	0.038
	123.4	0.03	...	27	26	37	89	-0.09	41.98	261.40	1053	5.62
U8357	9814	14.30	-12.91	0.24	< 0.22	2.71	5.04	> 0.04	-9.82	6.76	11.9	0.010
	130.9	0.03	22	48	74	63	97	-0.27	41.41	80.78	1212	16.98
U8387	6993	14.03	...	0.31	1.51	15.20	28.82	-0.69	-9.07	4.47	52.1	...
	93.2	0.04	...	39	44	85	148	-0.28	...	232.97	...	...
U8416	9137	15.19	...	<0.12	0.09	0.60	1.36	< 0.12	-10.44	2.51	6.7	...
	121.8	0.00	...	40	31	33	85	-0.36	...	16.88	...	...

TABLE 1—*Continued*

Name	V_0	B_T	log F(Hα)	$f_\nu(12)$	$f_\nu(25)$	$f_\nu(60)$	$f_\nu(100)$	log $\frac{f(12)}{f(25)}$	log F(IR)	L_B	L_{IR}/L_B	$L_{H\alpha}/L_B$
	D	A_B	W_λ(Hα)	σ	σ	σ	σ	log $\frac{f(60)}{f(100)}$	log $L_{H\alpha}$	L_{IR}	$L_{IR}/L_{H\alpha}$	$L_{H\alpha}$/area
(1)	(2)	(3)	(4)	(5)	(6)	(7)	(8)	(9)	(10)	(11)	(12)	(13)
U8454	6444	15.19	···	<0.25	0.27	1.84	3.42	<-0.03	-9.99	1.66	14.3	···
	85.9	0.30	···	···	···	···	···	-0.27	···	23.84	···	···
U8528/9	3065	12.16	···	0.31	0.99	7.02	15.47	-0.50	-9.37	4.79	4.6	···
	40.9	0.03	···	22	31	17	94	-0.34	···	22.25	···	···
U8584	17291	15.02	···	0.17	0.52	2.60	4.38	-0.49	-9.85	10.96	21.0	···
	230.5	0.05	···	42	52	46	100	-0.23	···	232.97	···	···
U8641/5	6688	12.78	-11.89	0.58	1.51	10.95	21.51	-0.42	-9.20	12.59	12.4	0.026
	89.2	0.01	···	40	75	60	58	-0.29	42.09	157.51	484	9.77
U8677/8	7687	13.57	···	0.23	0.22	1.58	5.26	0.02	-9.93	7.94	4.9	···
	102.5	0.00	···	32	32	39	172	-0.52	···	38.66	···	···
U8774	9849	14.13	-12.66	0.22	0.51	5.85	11.93	-0.37	-9.47	7.94	22.9	0.015
	131.3	0.03	···	27	43	46	66	-0.31	41.66	185.05	1531	46.77
U8849	6651	14.54	···	<0.14	< 0.11	0.20	1.39	···	-10.62	2.45	2.4	···
	88.7	0.00	···	46	38	45	75	-0.84	···	5.85	···	···
U8898/900	3560	12.06	···	<0.33	0.90	7.09	11.79	<-0.44	-9.42	6.92	3.9	···
	47.5	0.00	···	···	···	···	···	-0.22	···	26.75	···	···
U8929	8239	14.78	···	<0.15	< 0.15	0.44	1.53	···	-10.47	3.09	4.1	···
	109.9	0.03	···	50	49	42	134	-0.54	···	12.80	···	···
U8931/2	3838	13.62	-12.61	<0.08	< 0.07	0.76	2.30	···	-10.27	1.91	2.3	0.011
	51.2	0.00	···	27	24	38	134	-0.48	40.89	4.44	219	14.79
U8941	7733	14.13	-12.86	0.10	0.33	0.72	1.88	-0.52	-10.33	4.79	3.3	0.009
	103.1	0.00	···	32	29	40	110	-0.42	41.24	15.75	341	7.76
U9000/1	11186	14.78	···	<0.13	0.18	0.94	2.00	<-0.14	-10.25	5.50	7.0	···
	149.1	0.00	···	42	42	39	81	-0.33	···	38.66	···	···
U9102	7387	13.85	···	<0.14	< 0.17	1.40	2.57	···	-10.11	5.89	4.1	···
	98.5	0.03	···	45	58	50	131	-0.26	···	23.84	···	···
U9178	8891	15.11	-12.70	<0.08	< 0.08	0.23	0.80	···	-10.76	2.57	3.0	0.034
	118.5	0.00	···	25	28	20	96	-0.54	41.53	7.71	88	3.24
U9326/7	15916	15.11	···	0.14	0.23	1.49	2.48	-0.22	-10.10	9.12	12.4	···
	212.2	0.10	···	29	34	32	129	-0.22	···	111.51	···	···
U9425	10538	14.70	···	0.09	0.42	2.22	3.15	-0.67	-9.95	5.25	13.1	···
	140.5	0.00	···	28	32	30	84	-0.15	···	68.75	···	···
U9507	9530	14.21	-12.92	0.11	0.26	2.57	4.23	-0.37	-9.86	6.76	10.2	0.009
	127.1	0.00	···	31	36	27	76	-0.22	41.37	68.75	1138	0.89
U9525	8436	14.62	-12.37	<0.10	< 0.10	0.47	1.63	···	-10.45	3.72	3.9	0.046
	112.5	0.01	···	34	32	34	102	-0.54	41.81	14.04	84	5.01
U9580	8886	14.94	-12.62	<0.09	0.25	0.43	1.25	<-0.44	-10.53	3.16	4.1	0.034
	118.5	0.05	···	29	45	32	136	-0.46	41.62	13.10	121	4.37
U10033	3402	13.24	···	<0.25	0.54	4.06	7.31	<-0.33	-9.65	2.24	6.5	···
	45.4	0.06	···	···	···	···	···	-0.26	···	14.36	···	···
U10267	9081	13.89	-12.09	0.26	1.25	6.27	10.64	-0.68	-9.47	8.32	18.7	0.045
	121.1	0.00	···	22	26	38	98	-0.23	42.15	153.92	416	102.33
U10610	10307	14.70	-12.40	<0.07	0.16	0.85	2.43	<-0.36	-10.23	5.01	6.8	0.047
	137.4	0.00	···	22	29	24	60	-0.46	41.95	34.46	146	6.31
U10923	8045	14.13	-12.30	0.33	0.57	4.65	11.67	-0.24	-9.53	6.31	17.0	0.032
	107.3	0.21	27	22	19	25	75	-0.40	41.89	106.49	531	18.62
U11044	3066	14.70	-12.48	<0.08	< 0.10	0.37	1.10	···	-10.59	0.62	2.2	0.034
	40.9	0.36	···	27	34	30	103	-0.47	40.91	1.34	64	6.92
U11175	6496	14.10	-12.34	0.33	1.04	6.78	13.83	-0.50	-9.40	4.27	21.7	0.028
	86.6	0.22	···	20	16	24	62	-0.31	41.67	92.75	766	3.72
U11284	8823	14.94	-12.33	0.41	1.07	8.66	14.68	-0.42	-9.33	3.55	57.1	0.064
	117.6	0.19	···	···	···	···	···	-0.23	41.93	202.91	899	11.75
U11391	4811	13.32	-11.98	0.24	0.76	6.71	14.65	-0.50	-9.39	5.75	9.0	0.029
	64.1	0.42	41	19	22	40	75	-0.34	41.81	52.16	306	16.60
U11657/8	6013	14.21	···	<0.10	0.18	0.80	1.86	<-0.26	-10.31	3.47	2.9	···
	80.2	0.27	···	32	41	42	107	-0.37	···	9.94	···	···
U11664	···	15.51	···	<0.07	0.09	0.75	1.54	<-0.11	-10.36	···	···	···
	···	0.26	···	22	17	32	170	-0.31	···	···	···	···
U11673	14163	15.19	···	<0.07	< 0.10	0.80	2.15	···	-10.27	7.59	7.7	···
	188.8	0.25	···	22	35	45	145	-0.43	···	59.88	···	···
U11695	9863	14.46	-13.15	<0.06	< 0.11	0.65	1.70	···	-10.37	6.92	3.3	0.006
	131.5	0.19	6	19	37	47	158	-0.42	41.21	22.77	542	0.79
U11984/5	···	14.21	···	<0.34	0.52	6.47	13.08	<-0.18	-9.43	···	···	···
	···	0.28	···	···	···	···	···	-0.31	···	···	···	···
U12066	6030	14.38	-12.73	0.10	0.13	1.20	2.68	-0.11	-10.14	2.75	5.4	0.015
	80.4	0.18	21	29	38	27	101	-0.35	41.20	14.70	354	7.08

TABLE 1—*Continued*

Name	V_0 / D	B_T / A_B	log F(Hα) / W_λ(Hα)	$f_\nu(12)$ / σ	$f_\nu(25)$ / σ	$f_\nu(60)$ / σ	$f_\nu(100)$ / σ	log $\frac{f(12)}{f(25)}$ / log $\frac{f(60)}{f(100)}$	log F(IR) / log $L_{H\alpha}$	L_B / L_{IR}	L_{IR}/L_B / $L_{IR}/L_{H\alpha}$	$L_{H\alpha}/L_B$ / $L_{H\alpha}$/area
(1)	(2)	(3)	(4)	(5)	(6)	(7)	(8)	(9)	(10)	(11)	(12)	(13)
U12456/7	5132	12.80	···	0.17	0.21	1.68	5.80	-0.09	-9.89	8.51	2.2	···
	68.4	0.18	···	36	34	29	263	-0.54	···	18.51	···	···
N7592	7463	···	-12.27	0.32	1.10	6.92	12.17	-0.54	-9.42	···	···	···
	99.5	0.10	39	28	62	37	145	-0.25	41.83	116.76	667	48.98
U12578	2862	14.78	···	<0.08	< 0.20	0.32	< 0.40	···	<-10.81	0.41	< 1.7	···
	38.2	0.12	···	27	68	67	132	>-0.10	···	< 0.70	···	···
U12589	10323	15.19	-13.09	0.13	0.23	1.15	1.74	-0.25	-10.23	3.55	9.8	0.014
	137.6	0.11	11	35	58	69	69	-0.18	41.29	35.26	687	0.87
U12699/700	2965	12.79	-11.74	0.48	2.96	10.01	12.66	-0.79	-9.31	2.82	8.4	0.034
	39.5	0.16	51	75	81	59	82	-0.10	41.57	23.84	244	19.05
U12908/11	5043	13.42	-12.36	<0.12	< 0.09	0.27	1.04	···	-10.66	4.57	0.7	0.015
	67.2	0.16	···	39	30	30	106	-0.59	41.41	3.07	46	6.31
U12914/5	4785	12.40	-12.22	0.36	0.68	5.77	15.02	-0.28	-9.42	10.47	4.6	0.008
	63.8	0.15	15	29	43	41	190	-0.42	41.50	47.57	576	6.03

Col. (1): Galaxy identification by UGC, NGC, or Arp Atlas number.

Col. (2): Galactocentric velocity, V_0, corrected for the Sun's motion according to $V_0 = V + 250 \sin(l) \cos(b)$. Distance, D, in megaparsecs, assuming $H_0 = 75$ km s^{-1} Mpc^{-1}.

Col. (3): Total apparent blue magnitude, B_T, and blue extinction, A_B, in magnitudes.

Col. (4): Logarithm of the global Hα emission flux, F(Hα), in ergs s^{-1} cm^{-2}, and the Hα emission equivalent width, W_λ(Hα), in angstroms.

Cols. (5–8): *IRAS* flux densities, in Jy, obtained from ADDSCAN measurements or the *IRAS* Extragalactic Catalog. Uncertainty, σ, in mJy, is the rms noise in the ADDSCAN data and does not include the ~20% intrinsic calibration uncertainty in the *IRAS* data. Where no σ value is given, flux densities are from the Extragalactic Catalog.

Col. (9): Logarithm of the 12/25 μm and 60/100 μm flux density ratios.

Col. (10): Logarithm of the 40–120 μm flux, F(IR), in ergs s^{-1} cm^{-2}. Logarithm of the Hα luminosity, $L_{H\alpha}$, in ergs s^{-1}, corrected for Galactic reddening only such that $F_c(H\alpha) = F_{obs}(H\alpha) \times 10^{0.969E(B-V)}$, where $E(B-V) = A_B/4.1$.

Col. (11): Blue and infrared luminosities, in 10^9 $L_\odot$.

Col. (12): Infrared-to-blue and infrared-to-Hα luminosity ratios.

Col. (13): Hα-to-blue luminosity ratio, and Hα luminosity per unit area, $L_{H\alpha}$/area, in 10^{32} ergs s^{-1} pc^{-2}.

effort to place all of these data on a common scale, we have done the following. To make the optical data consistent with the *IRAS* data we have summed the Hα and blue magnitude data for each pair so that these data are also totals for each pair. All fluxes and luminosities in Table 1 are therefore totals for each interacting system, and all luminosity ratios have been computed by taking the ratio of these total luminosities.

Whenever comparisons are made between the data for the interacting and isolated galaxies we always refer to luminosities on a per-galaxy basis. We do this by dividing the luminosity values for the interacting pairs by a factor of 2 to account, in an average way, for the presence of two galaxies. This is reasonable at least in the case of optical luminosities since the majority of the interacting systems appear to be composed of pairs of galaxies of roughly comparable optical luminosity. Whether this is a reasonable approach for the infrared luminosity is not clear. For example, Telesco, Wolstencroft, and Done (1988) suggest that the distribution of IR flux between galaxies in pairs may be highly asymmetric, i.e., it is often the case that one galaxy in a pair is the dominant *IRAS* source. Whether this effect is real or merely an artifact of the *IRAS* point-source-finding algorithm is not clear at this time. We will investigate this in more detail in the future. If in fact one galaxy in each pair is the dominant source of the IR emission, then evenly dividing the total observed flux between the two galaxies will underestimate the luminosity of the stronger source and overestimate that of the weaker source. In the limiting case, where only one galaxy in a pair is an infrared source, then the actual L_{IR}/L_B ratio for the emitting galaxy could be a factor of 2 higher than that derived for the pair, while the nonemitting galaxy would have $L_{IR}/L_B = 0$.

Differences in the selection criteria for the samples of interacting and isolated galaxies could lead to self-imposed biases in our results. The one major difference between the two samples that we are aware of is the average distances of the galaxies. Since violently interacting galaxies are less common than isolated spirals, it is necessary to search to greater distances to obtain a large sample. As a result, the median distance of the interacting pairs is 89 Mpc, compared to a median distance of only 21 Mpc for the isolated spirals. While this difference in distance does not have a direct effect on our analysis, it does cause a bias in the luminosity of the sample members, since at greater distances we preferentially select systems that are intrinsically more luminous. A comparison of the blue luminosities of galaxies in the two samples shows that the interacting galaxies have a median $L_B \sim 1.9 \times 10^9$ $L_\odot$, while the median luminosity of the isolated spirals is 1.4×10^9 $L_\odot$; an increase of about 35% for the interacting galaxies. This difference in optical luminosity is taken into account where appropriate.

III. INFRARED PROPERTIES OF THE INTERACTING AND ISOLATED SYSTEMS

a) Infrared Luminosities

The infrared luminosities for our two samples of galaxies are given in Tables 1 and 2 and in the form of a histogram in Figure 1. The luminosity data in Figure 1 for the interacting pairs have been divided by a factor of 2 in order to approximate the contributions by the individual galaxies and to make a fair comparison with the data for the isolated galaxies (§ II). This results in median values of $L_{IR} = 1.3 \times 10^{10}$ $L_\odot$ and

TABLE 2

ISOLATED GALAXIES

Name	V_0	B_T	log F(Hα)	$f_\nu(12)$	$f_\nu(25)$	$f_\nu(60)$	$f_\nu(100)$	$\log \frac{f(12)}{f(25)}$	log F(IR)	L_B	L_{IR}/L_B	$L_{H\alpha}/L_B$
	D	A_B	W_λ(Hα)	σ	σ	σ	σ	$\log \frac{f(60)}{f(100)}$	log $L_{H\alpha}$	L_{IR}	$L_{IR}/L_{H\alpha}$	$L_{H\alpha}$/area
(1)	(2)	(3)	(4)	(5)	(6)	(7)	(8)	(9)	(10)	(11)	(12)	(13)
N278	883	11.51	-11.29	1.25	2.00	23.38	44.19	-0.20	-8.88	1.38	4.2	0.024
	11.8	0.73	27	...	...	...	...	-0.28	41.10	5.72	173	28.18
N337	1729	12.08	-11.64	<0.25	0.62	8.06	16.83	<-0.39	-9.32	2.14	3.7	0.021
	23.1	0.32	36	...	...	...	...	-0.32	41.24	7.89	174	6.46
N450	1852	12.50	-12.02	<0.11	0.22	2.46	5.04	<-0.30	-9.84	1.45	1.9	0.014
	24.7	0.17	28	...	...	...	...	-0.31	40.88	2.74	137	1.78
N681	1773	12.71	...	0.38	< 0.47	2.72	7.32	>-0.09	-9.74	0.93	3.4	...
	23.6	0.00	3	...	...	...	...	-0.43	...	3.14	...	...
N718	1885	12.50	...	<0.48	< 0.45	0.63	1.20	...	-10.45	1.38	0.5	...
	25.1	0.08	-3	...	...	...	...	-0.28	...	0.70	...	...
N949	773	12.55	-11.94	0.18	0.25	4.20	7.40	-0.14	-9.64	0.24	3.2	0.017
	10.3	0.17	15	...	...	...	...	-0.25	40.20	0.77	182	2.95
N1022	1500	12.20	-12.26	0.80	3.28	19.85	26.70	-0.61	-9.01	1.12	11.1	0.006
	20.0	0.04	6	...	...	...	...	-0.13	40.43	12.23	1748	1.62
N1058	675	12.15	-12.00	<0.32	< 0.25	2.47	8.93	...	-9.71	0.28	1.7	0.010
	9.0	0.23	15	...	...	...	...	-0.56	40.04	0.49	170	2.24
N1079	1346	12.22	...	<0.71	< 0.24	0.64	1.46	...	-10.41	0.85	0.5	...
	17.9	0.00	-1	...	...	...	...	-0.36	...	0.40	...	...
N1084	1398	11.22	-11.30	1.26	2.30	25.57	53.98	-0.26	-8.82	2.40	6.8	0.023
	18.6	0.05	30	...	...	...	...	-0.32	41.33	16.49	293	11.22
N1087	1535	11.55	-11.57	0.61	0.90	9.13	28.82	-0.17	-9.18	2.24	3.8	0.016
	20.5	0.11	26	...	...	...	...	-0.50	41.16	8.66	231	4.27
N1140	1484	12.85	-11.82	<0.25	0.43	2.99	4.76	<-0.24	-9.80	0.63	3.0	0.031
	19.8	0.11	60	...	...	...	...	-0.20	40.88	1.94	98	13.80
N1156	474	12.25	-11.76	<0.25	0.48	5.24	10.24	<-0.28	-9.52	0.19	2.0	0.016
	6.3	0.66	74	...	...	...	...	-0.29	40.08	0.38	120	4.79
N1357	1939	12.60	...	<0.25	< 0.40	1.02	4.72	...	-10.03	1.35	1.4	...
	25.9	0.10	3	...	...	...	...	-0.67	...	1.94	...	...
N1385	1390	11.65	-11.49	0.78	1.45	15.73	34.74	-0.27	-9.02	1.51	6.7	0.023
	18.5	0.00	34	...	...	...	...	-0.34	41.12	10.17	293	6.31
N1518	810	12.30	-11.89	<0.25	< 0.25	2.24	6.00	...	-9.83	0.30	1.9	0.016
	10.8	0.03	24	...	...	...	...	-0.43	40.26	0.55	113	2.57
N1637	640	11.50	-11.80	0.37	0.98	5.64	13.23	-0.42	-9.46	0.42	1.9	0.009
	8.5	0.12	12	...	...	...	...	-0.37	40.17	0.79	207	2.82
N1832	1784	12.10	-11.74	0.36	0.58	6.61	16.60	-0.21	-9.37	1.95	3.8	0.018
	23.8	0.18	21	...	...	...	...	-0.40	41.13	7.54	211	4.68
N2139	1633	12.05	-11.66	0.33	0.63	6.55	13.55	-0.28	-9.42	1.45	3.9	0.022
	21.8	0.00	34	...	...	...	...	-0.32	41.09	5.72	175	8.13
N2276	2630	11.98	-11.61	0.59	1.14	11.60	28.73	-0.29	-9.13	3.98	7.1	0.023
	35.1	0.00	31	...	...	...	...	-0.39	41.56	28.66	301	6.46
N2681	765	11.09	...	<0.35	0.59	6.96	10.95	<-0.23	-9.44	0.83	1.4	...
	10.2	0.09	-2	...	...	...	...	-0.20	...	1.19	...	...
N2763	1640	12.67	-12.03	0.16	0.18	2.20	6.20	-0.05	-9.82	0.95	2.3	0.016
	21.9	0.16	21	...	...	...	...	-0.45	40.77	2.22	147	3.55
N3185	1143	12.95	-12.82	<0.25	< 0.29	1.55	3.53	...	-10.02	0.34	2.0	0.003
	15.2	0.09	3	...	...	...	...	-0.36	39.65	0.69	597	0.55
N3310	1059	11.20	-11.03	1.25	4.66	32.96	40.79	-0.57	-8.80	1.35	7.4	0.043
	14.1	0.00	84	...	...	...	...	-0.09	41.35	9.94	170	12.88
N3389	1167	12.35	-11.90	0.22	0.40	3.80	9.60	-0.26	-9.61	0.60	3.1	0.016
	15.6	0.06	26	...	...	...	...	-0.40	40.58	1.85	188	3.24
N3504	1481	11.80	-11.58	1.05	3.74	18.91	32.06	-0.55	-8.99	1.55	7.9	0.021
	19.7	0.04	26	...	...	...	...	-0.23	41.10	12.51	379	6.76
N3955	1292	12.55	-12.05	0.56	0.78	7.89	17.07	-0.14	-9.33	0.66	6.6	0.014
	17.2	0.15	14	...	...	...	...	-0.34	40.54	4.34	488	1.78
N4027	1463	11.65	-11.60	0.54	0.96	10.15	27.30	-0.25	-9.17	1.78	4.5	0.017
	19.5	0.06	23	...	...	...	...	-0.43	41.07	8.08	260	5.37
N4152	2087	12.50	-11.97	0.32	0.53	4.13	9.20	-0.22	-9.60	1.74	3.5	0.016
	27.8	0.11	24	...	...	...	...	-0.35	41.02	6.13	220	3.72
N4394	890	11.74	...	<0.30	< 0.25	0.99	4.16	...	-10.07	0.58	0.6	...
	11.9	0.00	-1	...	...	...	...	-0.62	...	0.37	...	...
N4420	1571	12.71	-11.94	0.16	0.20	2.60	7.30	-0.10	-9.75	0.74	3.3	0.021
	20.9	0.01	30	...	...	...	...	-0.45	40.78	2.44	153	4.17
N4449	258	9.85	-10.71	1.63	3.95	32.00	66.20	-0.38	-8.73	0.28	2.5	0.026
	3.4	0.00	47	...	...	...	...	-0.32	40.44	0.69	96	13.49
N4504	847	11.92	-11.89	<0.25	< 0.33	1.41	5.02	...	-9.96	0.46	1.0	0.011
	11.3	0.04	20	...	...	...	...	-0.55	40.30	0.43	83	1.48

TABLE 2—*Continued*

Name	V_0	B_T	log F(Hα)	$f_\nu(12)$	$f_\nu(25)$	$f_\nu(60)$	$f_\nu(100)$	$\log \frac{f(12)}{f(25)}$	log F(IR)	L_B	L_{IR}/L_B	$L_{H\alpha}/L_B$
	D	A_B	W_λ(Hα)	σ	σ	σ	σ	$\log \frac{f(60)}{f(100)}$	log $L_{H\alpha}$	L_{IR}	$L_{IR}/L_{H\alpha}$	$L_{H\alpha}$/area
(1)	(2)	(3)	(4)	(5)	(6)	(7)	(8)	(9)	(10)	(11)	(12)	(13)
N4597	905	12.58	-11.95	<0.25	< 0.45	0.62	2.65	···	-10.27	0.28	0.9	0.018
	12.1	0.03	27	···	···	···	···	-0.63	40.30	0.24	47	1.55
N4602	2418	12.28	-12.15	0.54	0.50	5.02	13.20	0.03	-9.48	2.63	4.0	0.009
	32.2	0.03	12	···	···	···	···	-0.42	40.95	10.65	458	0.98
N4632	1604	12.22	-11.82	<0.37	< 0.35	3.92	10.48	···	-9.59	1.23	3.0	0.018
	21.4	0.03	25	···	···	···	···	-0.43	40.93	3.69	169	2.82
N4658	2239	12.74	-12.27	0.38	< 0.35	< 0.40	< 1.20	> 0.04	<-10.55	1.58	< 0.5	0.010
	29.9	0.10	14	···	···	···	···	···	40.78	< 0.79	< 50	2.14
N4775	1427	11.74	-11.80	<0.12	< 0.19	3.60	10.30	···	-9.61	1.51	1.8	0.012
	19.0	0.03	27	···	···	···	···	-0.46	40.84	2.80	153	5.75
N4781	1112	11.69	-11.76	0.50	0.53	7.40	17.60	-0.03	-9.34	1.02	3.1	0.012
	14.8	0.09	18	···	···	···	···	-0.38	40.68	3.14	253	2.63
N4790	1204	12.81	-12.09	<0.12	0.19	2.70	6.10	<-0.20	-9.78	0.44	3.0	0.016
	16.1	0.12	22	···	···	···	···	-0.35	40.43	1.34	190	4.68
N4808	668	12.56	-11.76	0.68	0.70	6.69	14.73	-0.01	-9.39	0.15	6.6	0.028
	8.9	0.00	32	···	···	···	···	-0.34	40.22	0.99	232	4.37
N4900	870	12.06	-11.64	0.34	0.47	5.39	11.86	-0.14	-9.49	0.41	3.3	0.023
	11.6	0.00	30	···	···	···	···	-0.34	40.57	1.37	142	7.59
N4941	522	11.90	-12.04	<0.25	< 0.58	1.31	3.95	···	-10.03	0.17	0.8	0.008
	7.0	0.01	9	···	···	···	···	-0.48	39.73	0.14	101	1.20
N5633	2464	12.90	-12.16	<0.27	0.33	2.66	7.53	<-0.09	-9.74	1.51	4.0	0.015
	32.9	0.00	17	···	···	···	···	-0.45	40.95	6.13	262	2.34
N5676	2268	11.68	-11.74	0.60	0.92	10.18	29.81	-0.19	-9.15	4.07	5.0	0.013
	30.2	0.03	16	···	···	···	···	-0.47	41.31	20.29	382	2.24
N5806	1357	12.30	-12.08	<0.25	< 0.44	2.63	7.96	···	-9.73	0.91	2.1	0.010
	18.1	0.15	11	···	···	···	···	-0.48	40.55	1.89	206	1.70
N5962	2046	12.10	-11.82	0.59	0.86	8.46	21.35	-0.16	-9.26	2.40	5.3	0.015
	27.3	0.10	18	···	···	···	···	-0.40	41.15	12.80	340	3.63
N5970	2035	12.15	-11.90	<0.34	0.34	2.64	9.23	< 0.00	-9.69	2.19	2.1	0.014
	27.1	0.07	18	···	···	···	···	-0.54	41.06	4.65	155	2.69
N6070	2058	12.35	-11.92	<0.31	0.41	4.31	12.86	<-0.12	-9.52	2.45	2.9	0.014
	27.4	0.36	18	···	···	···	···	-0.47	41.12	7.04	207	2.00
N6106	1543	12.80	-11.91	<0.25	< 0.25	1.49	4.85	···	-9.96	0.79	1.8	0.023
	20.6	0.22	30	···	···	···	···	-0.51	40.85	1.44	79	3.80
N6181	2517	12.50	-11.73	0.51	1.04	8.75	19.85	-0.31	-9.27	2.82	6.7	0.026
	33.6	0.23	28	···	···	···	···	-0.36	41.45	18.94	253	5.62
N6207	1048	12.15	-11.70	<0.25	0.40	4.38	11.27	<-0.20	-9.55	0.58	3.0	0.022
	14.0	0.05	26	···	···	···	···	-0.41	40.68	1.73	139	4.07
N6217	1593	11.86	-11.71	0.50	1.55	10.35	20.50	-0.49	-9.23	1.86	4.5	0.016
	21.2	0.14	21	···	···	···	···	-0.30	41.06	8.46	283	3.98
N6412	1564	12.32	-12.04	0.28	< 0.25	2.08	7.11	> 0.05	-9.80	1.23	1.7	0.011
	20.9	0.18	15	···	···	···	···	-0.53	40.72	2.12	156	3.31
I4662	290	11.76	-11.22	<0.25	1.05	8.13	11.36	<-0.62	-9.39	0.08	2.5	0.042
	3.9	0.27	38	···	···	···	···	-0.15	40.10	0.19	58	25.12
N6574	2504	12.85	-11.92	0.93	1.69	14.26	27.15	-0.26	-9.09	3.55	8.0	0.019
	33.4	0.83	20	···	···	···	···	-0.28	41.40	28.01	427	16.22
N6643	1754	11.74	-11.56	0.67	0.98	10.14	30.95	-0.17	-9.14	2.75	4.5	0.019
	23.4	0.22	24	···	···	···	···	-0.48	41.31	12.23	232	3.72
N7137	1951	13.05	-12.11	0.23	0.31	3.20	7.40	-0.13	-9.70	1.10	3.8	0.018
	26.0	0.30	18	···	···	···	···	-0.36	40.87	4.14	216	6.92
N7213	1738	11.18	···	0.64	0.75	2.54	8.28	-0.07	-9.73	3.72	0.9	···
	23.2	0.00	1	···	···	···	···	-0.51	···	3.14	···	···
N7217	1221	11.10	-11.79	0.47	< 0.25	4.78	18.22	> 0.27	-9.41	2.88	1.1	0.006
	16.3	0.42	4	···	···	···	···	-0.58	40.81	3.22	189	2.63
N7218	1782	12.55	-11.95	0.23	0.33	4.70	9.80	-0.16	-9.56	1.17	4.1	0.018
	23.8	0.08	19	···	···	···	···	-0.32	40.90	4.87	236	3.31
N7392	3210	12.65	-12.23	0.11	0.23	2.26	7.30	-0.32	-9.78	3.39	2.8	0.010
	42.8	0.05	8	···	···	···	···	-0.51	41.12	9.49	273	2.57
N7448	2427	12.15	-11.70	0.41	0.61	7.62	17.59	-0.17	-9.33	3.31	4.6	0.021
	32.4	0.14	30	···	···	···	···	-0.36	41.43	15.39	218	5.37
N7590	1484	12.20	-11.61	0.52	0.85	7.27	17.43	-0.21	-9.34	1.05	5.3	0.029
	19.8	0.00	39	···	···	···	···	-0.38	41.06	5.59	186	6.03
N7716	2734	12.95	-12.48	<0.25	< 0.35	0.67	2.08	···	-10.32	1.95	1.0	0.007
	36.5	0.11	7	···	···	···	···	-0.49	40.75	1.98	137	1.20
N7723	2018	11.85	-12.10	<0.38	0.53	4.11	10.42	<-0.14	-9.58	2.88	2.1	0.007
	26.9	0.08	7	···	···	···	···	-0.40	40.86	5.99	319	1.15

TABLE 2—*Continued*

Name	V_0 / D	B_T / A_B	log F(Hα) / W_λ(Hα)	$f_\nu(12)$ / σ	$f_\nu(25)$ / σ	$f_\nu(60)$ / σ	$f_\nu(100)$ / σ	$\log \frac{f(12)}{f(25)}$ / $\log \frac{f(60)}{f(100)}$	log F(IR) / log $L_{H\alpha}$	L_B / L_{IR}	L_{IR}/L_B / $L_{IR}/L_{H\alpha}$	$L_{H\alpha}/L_B$ / $L_{H\alpha}$/area
(1)	(2)	(3)	(4)	(5)	(6)	(7)	(8)	(9)	(10)	(11)	(12)	(13)
N7741	989	11.88	-11.83	<1.38	< 0.38	2.01	7.01	···	-9.81	0.71	1.2	0.012
	13.2	0.14	18	···	···	···	···	-0.54	40.52	0.83	96	1.82
N7742	1846	12.25	-12.10	<0.25	< 0.43	3.01	6.47	···	-9.75	1.70	2.0	0.009
	24.6	0.10	10	···	···	···	···	-0.33	40.78	3.37	214	3.63
N7743	1879	12.08	···	<0.25	< 0.42	0.96	2.50	···	-10.20	2.19	0.6	···
	25.1	0.18	2	···	···	···	···	-0.42	···	1.22	···	···

Col. (1): Galaxy identification by UGC, NGC, or Arp Atlas number.

Col. (2): Galactocentric velocity, V_0, corrected for the Sun's motion according to $V_0 = V + 250 \sin(l) \cos(b)$. Distance, D, in megaparsecs, assuming $H_0 = 75$ km s^{-1} Mpc^{-1}.

Col. (3): Total apparent blue magnitude, B_T, and blue extinction, A_B, in magnitudes.

Col. (4): Logarithm of the global Hα emission flux, F(Hα), in ergs s^{-1} cm^{-2}, and the Hα emission equivalent width, W_λ(Hα), in angstroms.

Cols. (5–8): *IRAS* flux densities, in Jy, obtained from ADDSCAN measurements or the *IRAS* Extragalactic Catalog. Uncertainty, σ, in mJy, is the rms noise in the ADDSCAN data and does not include the ~20% intrinsic calibration uncertainty in the *IRAS* data. Where no σ value is given, flux densities are from the Extragalactic Catalog.

Col. (9): Logarithm of the 12/25 μm and 60/100 μm flux density ratios.

Col. (10): Logarithm of the 40–120 μm flux, F(IR), in ergs s^{-1} cm^{-2}. Logarithm of the Hα luminosity, $L_{H\alpha}$, in ergs s^{-1}, corrected for Galactic reddening only such that $F_c(H\alpha) = F_{obs}(H\alpha) \times 10^{0.969E(B-V)}$, where $E(B-V) = A_B/4.1$.

Col. (11): Blue and infrared luminosities, in $10^9\ L_\odot$.

Col. (12): Infrared-to-blue and infrared-to-Hα luminosity ratios.

Col. (13): Hα-to-blue luminosity ratio, and Hα luminosity per unit area, $L_{H\alpha}$/area, in 10^{32} ergs s^{-1} pc^{-2}.

$3.1 \times 10^9\ L_\odot$ for the interacting and isolated galaxies, respectively (Table 3); more than a factor of 4 increase in IR luminosity for the interacting galaxies. However, since we know that the median optical luminosity of the interacting galaxies is higher than that of the isolated galaxies this is not a fair comparison. If we instead look at the ratio of infrared-to-optical luminosity we obtain a more appropriate comparison of the two samples. We find that the median values of L_{IR}/L_B[6] for the interacting and isolated galaxies are 5.6 and 3.0, respectively (see Fig. 1*b* and Table 3). Thus, by this measure, interactions are producing an approximate doubling of infrared luminosity.

The difference in median values of L_{IR} and particularly L_{IR}/L_B for the interacting and isolated galaxies is due in part to a shift in distributions, and also an excess of interacting systems with high IR luminosities which have no counterparts in the sample of isolated galaxies. Only one isolated galaxy has $L_{IR}/L_B > 10$, whereas 33% (30 out of 90) of the interacting systems have $L_{IR}/L_B > 10$. Notice in particular that seven interacting systems have $L_{IR}/L_B \geq 35$. An analysis of other available data for these seven systems indicates that they form a special, uniform group of objects. We will discuss them in more detail later (§ V*a*).

b) *Infrared Colors*

Infrared colors of the interacting and isolated galaxies are given in Tables 1 and 2, and are also presented in the form of a histogram in Figure 2 and in a color-color plot in Figure 3. These figures include data for only those objects that were detected in each of the wavelength bands that are plotted. As shown previously by others (e.g., Helou 1986) the galaxies spread out along a band in the $R(12/25) = f_\nu(12\ \mu\text{m})/f_\nu(25\ \mu\text{m})$ versus $R(60/100) = f_\nu(60\ \mu\text{m})/f_\nu(100\ \mu\text{m})$ color-color plot such that the larger their $R(12/25)$, the smaller their $R(60/100)$. As can be seen from Figures 2 and 3 the interacting and isolated galaxies span much of the same range in infrared colors. There are, however, interesting differences in the color distributions of the two samples. First, the sample of interacting galaxies has slightly higher median $R(60/100)$ and markedly lower median $R(12/25)$ values than the isolated galaxies (see Table 3). The positions of the mean colors of the isolated galaxies and the interacting pairs are marked in Figure 3 by the letters "I" and "P," respectively. For dust emissivity proportional to frequency, the median $R(60/100)$ colors of the two samples correspond to dust temperatures of 32 and 34 K.

The shapes of the distributions of IR colors for the two samples are also quite different. Although the colors of galaxies in the two samples span similar ranges, the colors of the isolated galaxies are more narrowly concentrated than are the

[6] Galactic blue luminosities are based on standard optical definitions. Thus we derive L_B from the in band flux via $f_B = \text{dex}(-0.4B_T - 5.19)$ ergs s^{-1} cm^{-2} which assumes the Johnson B response function. Others have adopted quasi-bolometric fluxes given by $f_B = \lambda_B \times f_\lambda(4400\ \text{Å})$ ergs s^{-1} cm^{-2}. The L_B on this latter system are a factor of 4.7 times larger than that used here, and consequently result in much lower L_{IR}/L_B values.

TABLE 3

MEDIAN PROPERTIES

Parameter	Interacting Galaxies[a]	Isolated Spirals
Radial velocity (km s^{-1})	6688	1535
Distance (Mpc)	89.2	20.5
L_B ($L_\odot$)	1.9×10^9	1.4×10^9
$L_{H\alpha}$ (ergs s^{-1})	1.7×10^{41}	7.2×10^{40}
W_λ(Hα) (Å)	27.3	21.0
L_{IR} ($L_\odot$)	1.3×10^{10}	3.1×10^9
L_{IR}/L_B	5.6	3.0
$L_{IR}/L_{H\alpha}$	484	206
$L_{H\alpha}/L_B$	0.015	0.017
log [f_ν(12 μm)/f_ν(25 μm)]	−0.42	−0.21
log [f_ν(60 μm)/f_ν(100 μm)]	−0.33	−0.39
νf_ν(25 μm)/νf_ν(B)	0.63	0.16
νf_ν(60 μm)/νf_ν(B)	0.95	0.53

[a] Luminosities for the interacting pairs are per galaxy, computed by dividing the total for each pair by two.

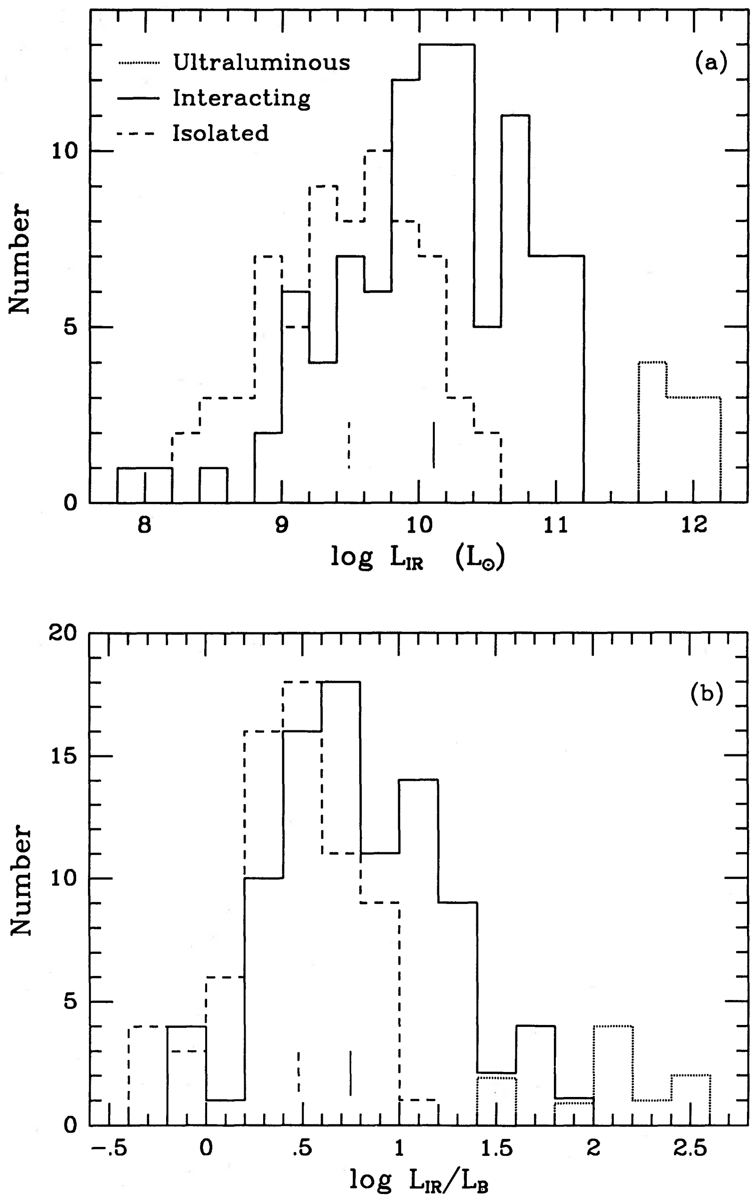

FIG. 1

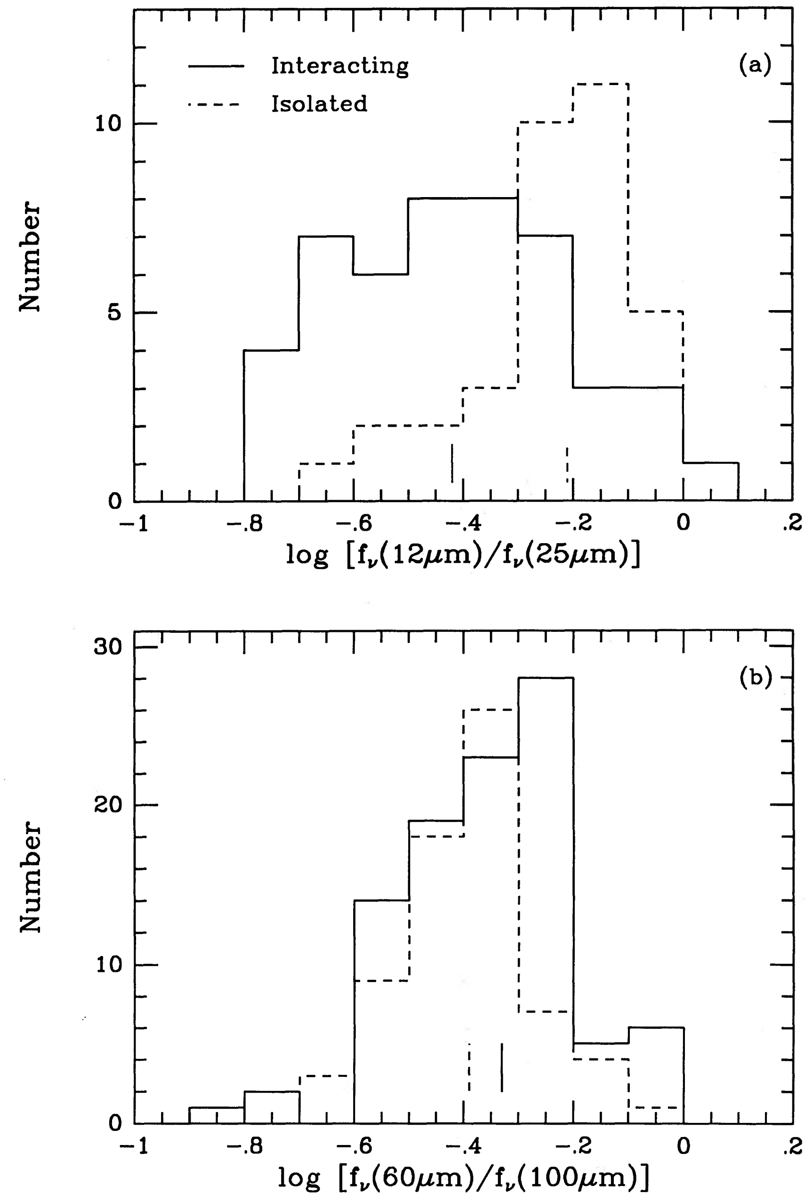

FIG. 2

FIG. 1.—Histograms of far-infrared luminosity and infrared-to-blue luminosity ratio for the interacting and isolated galaxy samples in this study, and also, for comparison, the ultraluminous *IRAS* systems from Sanders *et al.* (1988). In the L_{IR} diagram luminosities of the interacting pairs have been divided by a factor of 2 to account, on average, for the presence of two galaxies. The total pair luminosities have been used to compute L_{IR}/L_B. Vertical lines indicate the median values of the distributions. Upper limits are not included.

FIG. 2.—Histograms of $R(12/25)$ and $R(60/100)$ colors for the interacting and isolated galaxy samples. Vertical lines indicate the median values of the distributions. Upper limits are not included.

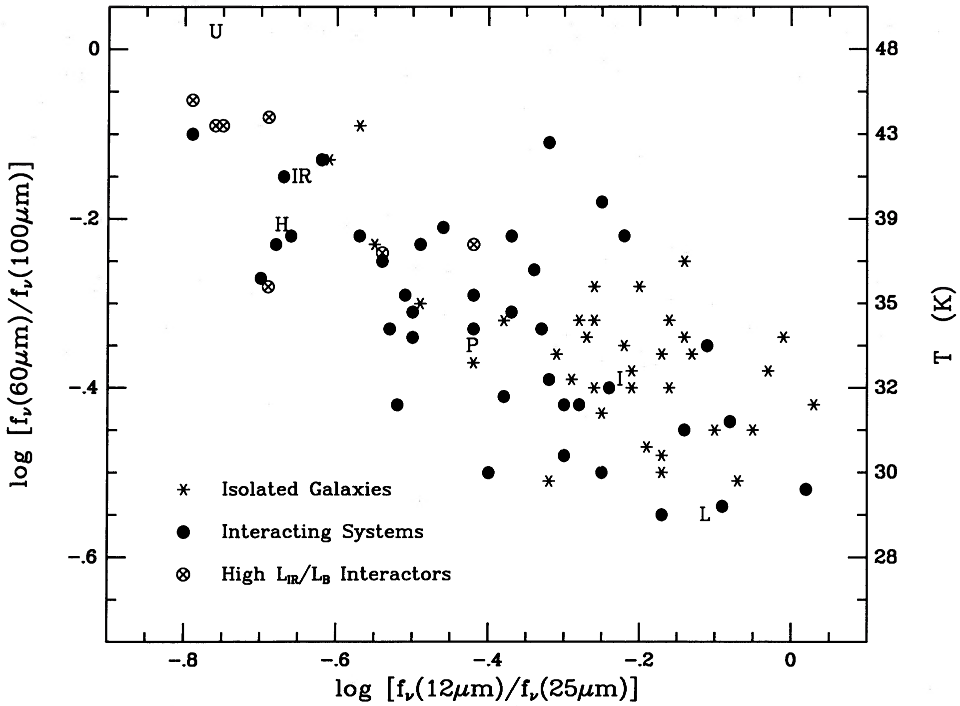

FIG. 3.—R(60/100) vs. R(12/15) color-color plot for the interacting and isolated galaxy samples. Dust temperatures shown along the right vertical axis are based on an assumed grain emissivity proportional to frequency. Letters denoted the mean colors of various samples: "L"—low SFR interactors; "I"—all isolated galaxies; "P"—all interacting pairs; "H"—high SFR interactors; "IR"—high L_{IR}/L_B interactors; and "U"—Sanders *et al.* sample of ultraluminous systems.

colors of the interacting galaxies. This effect is most apparent in the distribution of R(12/25) (Fig. 2*a*). Almost 80% of the isolated galaxies have R(12/25) colors that lie within a range of 0.3 around the peak of their distribution, but only $\sim$50% of the interacting pairs have R(12/25) values within an equal-sized range around the peak of their distribution. The IR properties of the isolated galaxies are much more uniform from galaxy to galaxy than those of the interacting systems.

There is a correlation between L_{IR}/L_B and both R(12/25) and R(60/100) for the two samples of galaxies, in the sense that L_{IR}/L_B increases with increasing R(60/100) and decreases with increasing R(12/25) (Fig. 4). Because of the amount of scatter in these relations, the correlations are much less obvious when examining only the sample of isolated galaxies since they do not span as large a range in IR color or L_{IR}/L_B. De Jong *et al.* (1984) also found a correlation between L_{IR}/L_B and R(60/100) for RSA galaxies and noted that this indicates that galaxies with high color temperatures emit a much larger fraction of their total luminosity in the infrared than do galaxies with low color temperatures. They went on to suggest that there are two infrared components in a galaxy: one (see Jura 1982) due to interstellar dust distributed throughout the disk which reradiates a small fraction of the general interstellar radiation field at a color temperature of 25–30 K; and another due to interstellar dust associated with H II regions and molecular clouds which reradiates the stellar radiation of recently formed massive stars at a color temperature of $\sim$50 K (see also Helou 1986; Persson and Helou 1987). When the SFR in a galaxy is high, the warmer component increases in importance as more, approximately 50 K radiation due to massive stars embedded in molecular clouds is emitted. Thus it is assumed that the relative intensity of star formation increases as shown in Figure 4, from left to right. We test this assumption below.

IV. COMPARISON OF OPTICAL AND INFRARED INDICATORS OF STAR FORMATION

Using the available optical data for the interacting galaxies (Bushouse 1986*a*, 1987) and for the isolated galaxies (Kennicutt and Kent 1983) we can compare the classical optical indicators of star formation with the infrared properties of the galaxies and also intercompare the results for the two different samples. The optical indicators of star formation include L_B, $L_{H\alpha}$, $L_{H\alpha}$/area (i.e., a measure of the star-formation rate per unit area), and $W_\lambda(H\alpha)$ (the Hα emission-line equivalent width), or, equivalently, the ratio $L_{H\alpha}/L_B$. Infrared emission properties that we will use for comparison are L_{IR}, L_{IR}/L_B, $L_{IR}/L_{H\alpha}$, and the colors R(12/25) and R(60/100). The reasoning behind these choices of optical and infrared parameters and what properties of the galaxies we expect them to measure are outlined below.

$L_{H\alpha}$ measures the flux of Lyman continuum photons and thus the populations of hot, young stars. Since most of the contribution to $L_{H\alpha}$ must come from stars with main-sequence lifetimes less than or equal to 10^7 years, Hα observations in principle provide an estimate of very recent star formation in a galaxy. This approach has been successfully adopted by several groups including Gallagher, Hunter, and Tutukov (1984; GHT), Hunter and Gallagher (1986), Israel (1980), and Kennicutt (1983). The ratio $L_{H\alpha}$/area thus measures the star-formation rate per unit area or the intensity of star formation within galaxies. To compute this parameter we divide the total Hα luminosity of a galaxy by the area of the galaxy as determined from its optical size. The blue luminosity, L_B, of a galaxy can be used to estimate the star formation rate (SFR) averaged over the past $\sim 3 \times 10^9$ yr (GHT). Therefore the luminosity ratio $L_{H\alpha}/L_B$ (or alternatively W_λ[Hα]) essentially measures the ratio of recent to more long-term star formation in a galaxy and thus provides an estimate of the relative "burstiness" of star-formation activity. Note, however, that measures of SFR based on Hα emission and blue luminosity are sensitive to the effects of dust.

In the past, L_{IR} has been assumed to measure the current SFR. Helou (1986) and Persson and Helou (1987), however, argue that L_{IR} has contributions originating both from dust heated by the hot massive star component of a galaxy and from diffusely heated dust in the general interstellar medium (§ III*b*). In any case, the amount and distribution of dust will be a factor in determining the emergent IR flux. We assume here that the IR flux is some measure of recent star-formation activity and we will probe this assumption by comparisons with the optical indicators of star formation.

The infrared-to-blue luminosity ratio, L_{IR}/L_B, is a measure of the infrared luminosity normalized to the size (i.e., stellar content) of a galaxy. Likewise, the ratio $L_{IR}/L_{H\alpha}$ is a measure of the infrared luminosity normalized to the number of (unobscured) massive stars in a galaxy. The IR colors, $R(12/25)$ and $R(60/100)$, are a measure of the dust temperature. All of these parameters will depend on the amount of dust and its distribution, as well as the heating rate of the dust due to both massive stars and the ambient interstellar radiation field. The sample of interacting galaxies has a median $L_{IR}/L_{H\alpha}$ that is a factor of 2.6 larger than that for the isolated galaxies (see Table 3). This suggests that star formation in the interacting galaxies may be occurring in more embedded environments.

In Figure 5 we plot the FIR luminosity of galaxies in the two samples against their Hα and blue luminosities. The correlation between FIR and Hα luminosity is good for both samples, although the interacting galaxies show considerably more scatter from the mean relation than the isolated galaxies. Figure 5*b* shows that there is also a good correlation between FIR and blue luminosity with approximately equal scatter in both samples. The factor of 2 differences in the medians of both L_{IR}/L_B and $L_{IR}/L_{H\alpha}$ for the two samples is less than the amount of scatter in both relations and therefore the offsets are not readily apparent in these diagrams. These same correlations

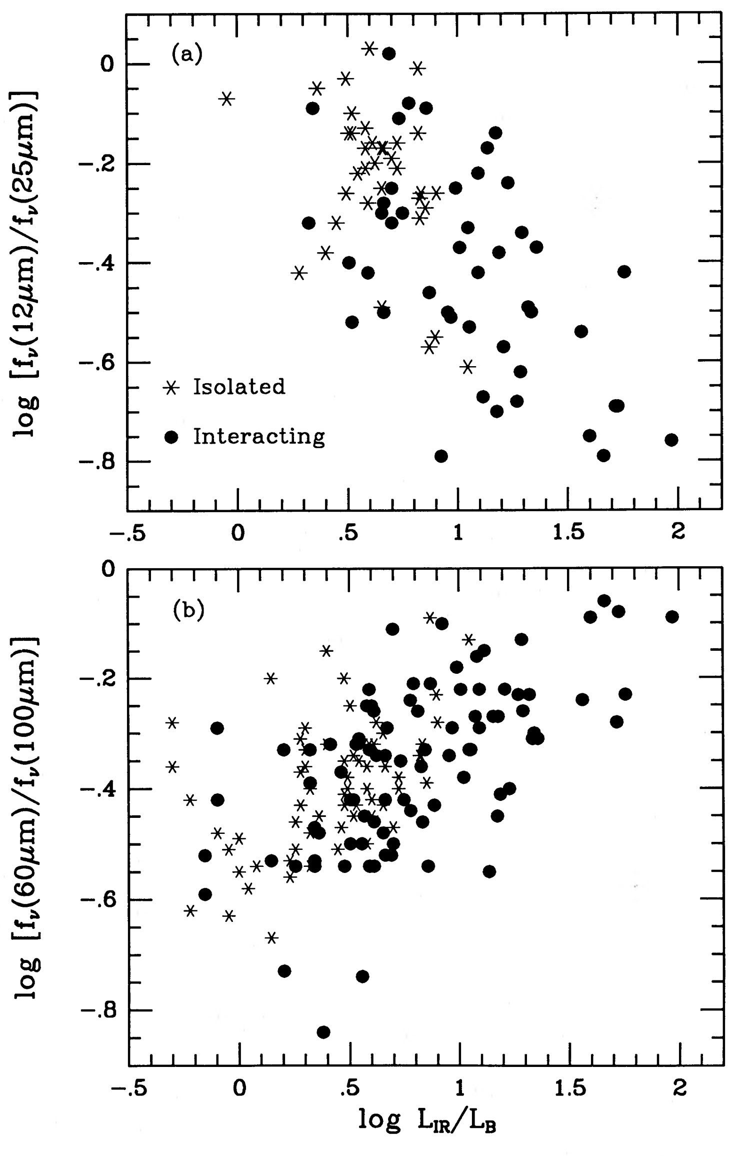

FIG. 4.—The infrared-to-blue luminosity ratio vs. $R(12/25)$ and $R(60/100)$ infrared colors for the interacting and isolated galaxy samples

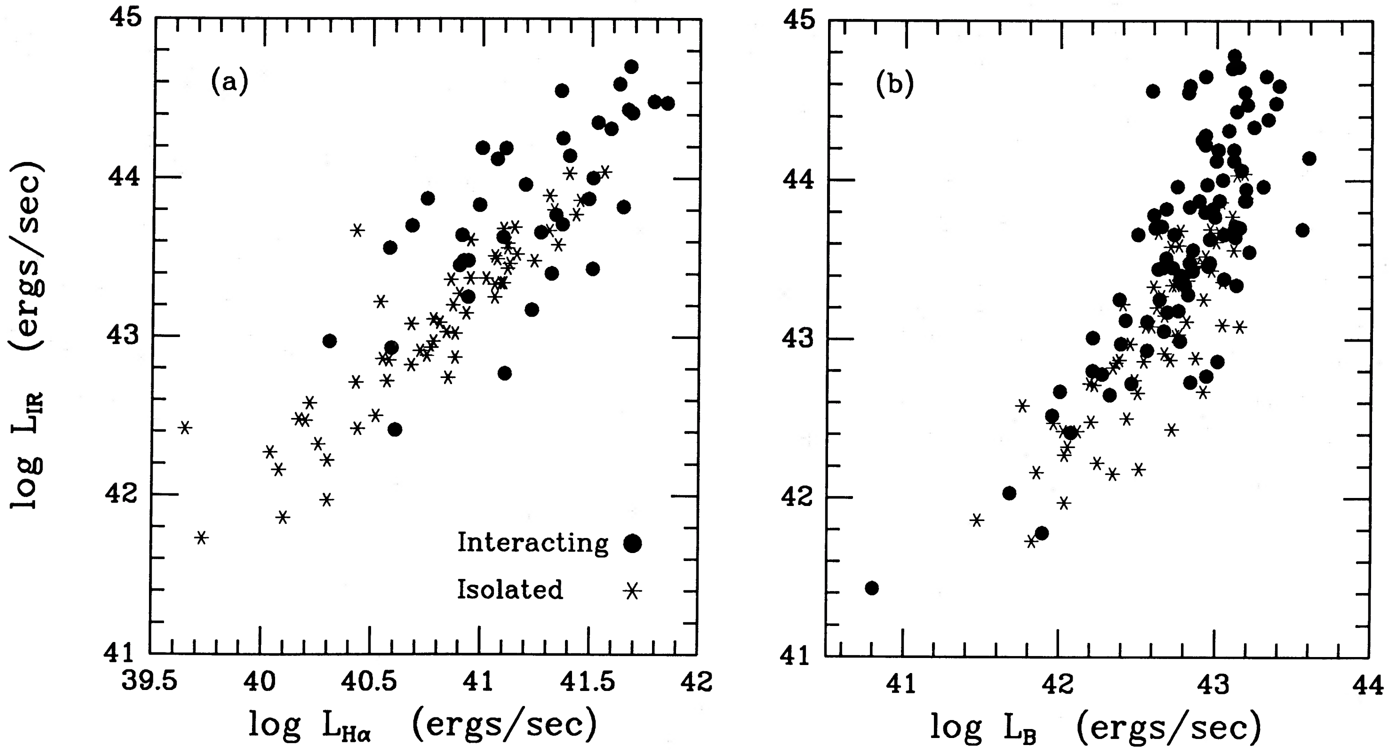

FIG. 5.—Infrared luminosity vs. Hα and blue luminosities for the interacting and isolated galaxy samples. Values of $L_{H\alpha}$ and L_B for the interactors are one-half the total for each pair.

still exist when all data in these figures are normalized by the size of the galaxies or when observed fluxes are plotted instead of luminosities.

Notice that the correlation between L_{IR} and L_B does not appear to be linear, at least for the interacting systems. L_{IR} appears to rise faster than L_B, especially at the higher values of L_B. Figure 6 shows L_{IR}/L_B plotted against L_B and it is clear from this diagram that the average infrared-to-blue luminosity ratio does in fact increase as a function of L_B for the interacting galaxies (see also Feigelson, Isobe, and Weedman 1987; Rieke and Lebofsky 1985). This diagram suggests two interesting points. First, as noted previously (§ III*a*), there are no isolated galaxies, of any optical luminosity, with $L_{IR}/L_B \gg 10$, whereas fully one-third of the interacting systems have $L_{IR}/L_B > 10$ and several have $L_{IR}/L_B > 30$. Therefore it is likely that galaxy-galaxy interactions are a necessary requirement for significant enhancements in infrared luminosity. Second, there appears to be a cutoff luminosity at $L_B \sim 10^9\ L_\odot$, below which no systems show a significant enhancement in infrared luminosity. Above this level, many interacting systems have $10 \leq L_{IR}/L_B \leq 100$. This result is consistent with Smith *et al.* (1987) who find that galaxies of low blue luminosity are not strong infrared emitters.

The fact that the FIR, Hα, and blue light from the galaxies correlate with one another indicates, first of all, that these three observables all scale with the overall size of a galaxy, at least to first order. Furthermore, if these three quantities represent a sampling of the average SFR over different periods of time in the past, then this must mean that the galaxies are evolving at roughly constant rates (GHT; Kennicutt 1983). The fact that the interacting galaxies show more scatter in these relations is consistent with the assumption that they have experienced more nonequilibrium star-formation activity in the recent past than the isolated galaxies.

Because the total FIR, Hα, and blue luminosities correlate with one another it is more appropriate to examine luminosity ratios and colors in order to look for relationships between optical SFR indicators and infrared parameters. In both samples L_{IR}/L_B, $R(12/25)$, and $R(60/100)$ correlate weakly with $L_{H\alpha}$/area, in the sense that average values of L_{IR}/L_B and $R(60/100)$ increase and $R(12/25)$ decreases as $L_{H\alpha}$/area increases (Fig. 7). These are not at all tight correlations, as individual values scatter up to an order of magnitude in any parameter. However, there is significantly less scatter in the relationship between $L_{H\alpha}$/area and L_{IR}/L_B for the isolated galaxies than there is for the interacting galaxies.

There is essentially no correlation between $L_{IR}/L_{H\alpha}$ and either $L_{H\alpha}$/area or the IR colors for both samples of galaxies. $L_{H\alpha}/L_B$ ratios (or alternatively W_λ[Hα]) for the galaxies also show little relationship with IR properties. There is only a weak positive relationship between $L_{H\alpha}/L_B$ (or W_λ[Hα]) with L_{IR}/L_B and, once again, the scatter is less for the isolated galaxies than for the interacting systems.

It appears, therefore, that the luminosity ratio L_{IR}/L_B and the infrared colors $R(12/25)$ and $R(60/100)$ come the closest to being related to optical indications of current star-formation activity as measured by $L_{H\alpha}$/area. These results are consistent with the earlier suggestions that the contribution by massive young stars to the total FIR flux of a galaxy becomes increasingly important as the overall massive star content of a galaxy increases. In this circumstance, the increased radiation from massive stars raises the dust temperature and hence reradiation from the warm dust contributes more heavily to the integrated 25 μm and 60 μm flux from the galaxy. This has the

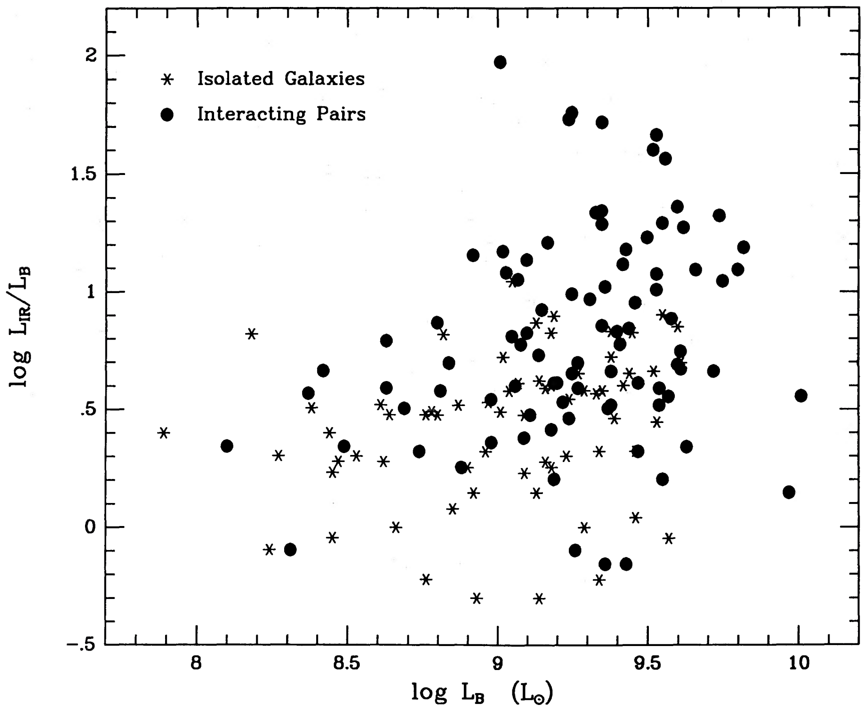

FIG. 6.—Infrared-to-blue luminosity ratio vs. blue luminosity for the interacting and isolated galaxy samples. Values of L_B used in computing L_{IR}/L_B for the interactors are the total for each pair, while the value of L_B plotted on the x axis is one-half the total for each pair.

effect of raising the observed $R(60/100)$ flux ratio and lowering the observed $R(12/25)$ flux ratio. The fact that the IR parameters correlate better with indicators of the absolute level of star-formation activity than with quantities such as $L_{H\alpha}/L_B$ and $W_\lambda(H\alpha)$, which measure the ratio of present to past star formation, is also consistent with this reasoning since the dust heating rate will depend more closely on the absolute number of massive stars that are present at any given time.

V. COMPARATIVE ANALYSIS OF VARIOUS SUBSAMPLES OF THE INTERACTING SYSTEMS

The sample of interacting galaxies consists of objects that span a large range in optically indicated levels of star-formation activity. This has been well documented by Bushouse (1986*a*, *b*, 1987). In this section we explore mean optical and infrared properties for five subgroups of the sample of interacting galaxies in a further attempt to determine to what extent IR emission is directly related to star-formation activity. Four of these subgroups are chosen to represent a particular optical quality related to star-formation activity, and the fifth is a group of objects with extreme L_{IR}/L_B values. We also include a comparison with the sample of ultraluminous *IRAS* systems studied by Sanders *et al.* (1988), as well as other samples of binary and interacting galaxies that have been studied via *IRAS* data.

As we do not have *IRAS* data for the individual galaxies within the interacting pairs it is impossible to compare the optical and *IRAS* data on a galaxy-by-galaxy basis. The optical properties of the two galaxies in any given pair can often be very dissimilar, thus in some instances we cannot compare the *IRAS* data with the combined optical data for the galaxies within a pair in a reliable way. Therefore in this analysis we are careful to select only pairs containing two galaxies with similar optical properties. Mean optical and infrared properties of these subgroups are presented in Table 4 and a list of the members of each subgroup is given in Table 5.

TABLE 4

MEAN PROPERTIES OF SUBSAMPLES

Sample	L_{IR}[a] ($10^9 L_\odot$)	L_B[a] ($10^9 L_\odot$)	L_{IR}/L_B	$L_{H\alpha}/L_B$	$\log \frac{f(12\ \mu m)}{f(25\ \mu m)}$	$\log \frac{f(60\ \mu m)}{f(100\ \mu m)}$	T_{dust}[b] (K)
Interacting: Low SFR	12.	3.8	2.5	0.008	−0.12	−0.55	29
Interacting: High SFR-Low IR	1.	0.4	2.5	...	...	−0.32	35
Isolated Spirals: All	6.	1.5	3.4	0.017	−0.23	−0.39	33
Interacting: Disk SF	36.	3.9	9.3	0.029	−0.43	−0.35	34
Interacting: All	29.	2.3	11.0	0.023	−0.43	−0.35	34
Interacting: High SFR	34.	1.4	14.2	0.031	−0.68	−0.21	38
Interacting: High L_{IR}/L_B	118.	2.4	54.0	0.051	−0.66	−0.15	41
Ultraluminous *IRAS* Galaxies[c]	766.	8.5	162.0	...	−0.77	+0.02	49

[a] Infrared and blue luminosities for interacting systems are per galaxy, computed by dividing the pair total by two.
[b] Dust temperature computed from the 60/100 μm flux ratio assuming emissivity proportional to frequency.
[c] From Sanders *et al.* (1988).

a) Subsamples with Extreme Values of Nuclear SFR

We have formed two groups of interacting galaxies, one of which is composed of galaxies that exhibit optical evidence of high-current SFRs, and the other is made up of interacting pairs that show little or no optical evidence of star-formation activity. The optical data that we have used to estimate current levels of star-formation activity are nuclear region (~2 kpc) spectra which are available for many of the interacting galaxies from Bushouse (1986*a*). High SFR pairs are those in which both galaxies have optical spectra containing strong H II region-like emission features and either a featureless continuum or one that is dominated by intermediate-age A–F type stars suggesting a high relative population of young stars. An example of one such member of the high SFR group is UGC 7905 and the spectrum of the southern component of this pair is shown in Figure 8. Low SFR systems are those that have optical spectra with either only a few very weak emission lines (e.g., [O II] λ3727 and/or Hα) or no detectable emission lines at all, and have an elliptical galaxy-like stellar continuum domi-

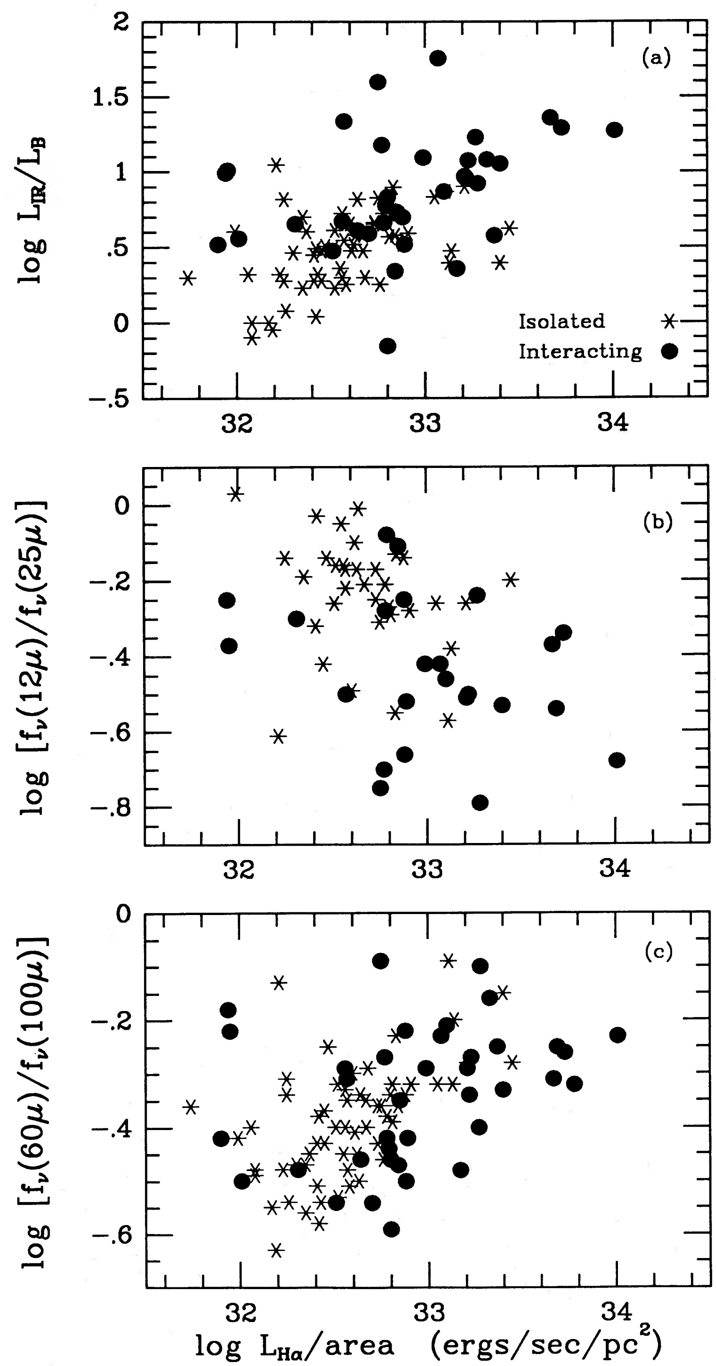

FIG. 7.—The Hα luminosity per unit area, $L_{H\alpha}$/area, plotted versus L_{IR}/L_B, and $R(12/25)$ and $R(60/100)$ infrared colors for the interacting and isolated galaxy samples.

TABLE 5

SUBGROUPS OF THE INTERACTING SYSTEMS

High L_{IR}/L_B	High SFR[a]	Low SFR	Disk SF
UGC 4509	Arp 248	UGC 11673	UGC 8641/5
UGC 11284	Arp 252	UGC 7277	NGC 4038/9
NGC 1614	NGC 1614	UGC 480	UGC 11391
UGC 8387	UGC 6471/2	UGC 8849	UGC 12914/5
UGC 6471/2	UGC 8335	UGC 717/9	
UGC 8335	UGC 10267	UGC 2320	
UGC 4881	UGC 12699	Arp 100	
	UGC 10033	UGC 3031/2	
	UGC 7905	UGC 12908/11	
	UGC 2992	Arp 250	
	UGC 4757*		
	UGC 7910*		
	UGC 3737*		
	UGC 8315*		
	UGC 993*		
	UGC 7891*		

[a] Objects in the high SFR group marked with an asterisk are interacting systems that have optical signs of high SFRs but have low levels of infrared emission.

nated by older G–M type stars. An example of a low SFR galaxy is UGC 3032 (Fig. 8).

Since we are relying on spectra of the near-nuclear regions only for defining the level of star-formation activity in these galaxies we must of course be careful that our results are not confused by unknown activity in the outer disk regions of the galaxies. Bushouse (1987) has determined that the majority of current star-formation activity is in fact taking place within the near-nuclear regions of the interacting galaxies and only rarely do the galaxies have any significant amount of star formation taking place in the outer disk regions. Therefore it is highly unlikely that the objects chosen for their low nuclear-region SFRs have any significant amount of star formation taking place outside of the regions sampled by the optical spectra. Furthermore, for those objects which also have Hα emission-line images available, we have confirmed that there are no obvious signs of significant star-formation activity in their outer regions.

The IR properties of the galaxies in the high and low SFR groups are remarkably different. First, the mean L_{IR}/L_B ratios

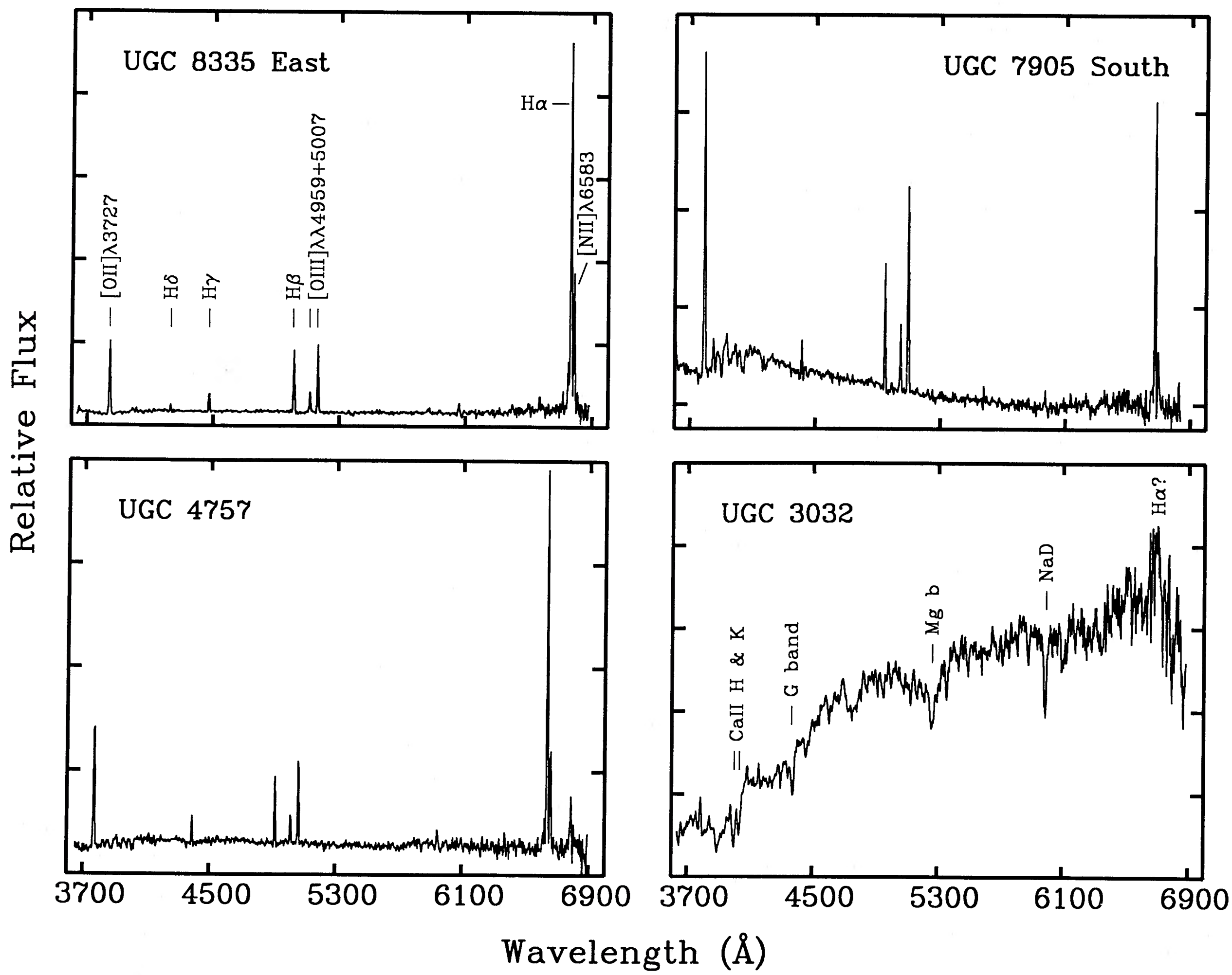

FIG. 8.—Nuclear region optical spectra for representative galaxies with different infrared and star-formation characteristics (§ V). UGC 8335 is a member of both the high L_{IR}/L_B and the high SFR subsamples and has a very strong H II region-like emission-line spectrum and an almost featureless continuum. UGC 7905 is a member of the high SFR subsample and also shows strong H II region-like emission features superposed on a very blue continuum, which is indicative of the presence of many hot, massive stars. UGC 4757 is one of the high SFR galaxies that has lower than normal infrared emission. Note the great similarity between the spectrum of this object and UGC 8335 East, which indicates that both galaxies are experiencing similar levels of star-formation activity, yet their infrared emission properties are vastly different. UGC 3032 is a member of the low SFR subsample and shows no obvious emission lines and a stellar continuum characteristic of old populations.

are 14 and 2.5 for the high and low SFR galaxies, respectively. This puts the value for the high SFR group above the mean for the interacting galaxy sample as a whole ($L_{IR}/L_B = 11$), whereas the mean for the low SFR group is somewhat lower than that of the isolated galaxies ($L_{IR}/L_B = 3.0$). We find even greater differences in the IR colors of the two groups (Table 4). The positions of the mean colors of the high and low SFR groups are marked by the letters "H" and "L," respectively, in Figure 3. The $R(60/100)$ colors correspond to mean dust temperatures of 38 K and 29 K for the high and low SFR groups, respectively. These results strengthen our conclusion (§ IV) that both the L_{IR}/L_B ratio and infrared colors are good indicators of current star-formation activity in galaxies.

b) *High SFR, Low IR Emission Systems*

Within the subsample of high SFR interacting galaxies discussed above there are a few galaxies which, on the basis of their optical spectra, have high nuclear region SFRs but have remarkably low IR luminosities as compared to both the interacting and isolated galaxy samples. These objects are marked in the list of high SFR systems in Table 5. The mean L_{IR}/L_B ratio for these objects is the same as that for the low SFR group discussed in the previous section. The mean $R(60/100)$ color of these objects, however, is comparable to the mean value for the whole interacting galaxy sample. So even though the level of infrared emission is very low, the color temperatures are still moderately enhanced relative to isolated galaxies. The optical spectrum of one of these objects, UGC 4757, is shown in Figure 8. Notice the great similarity between this spectrum and that of UGC 8335, which is an object with a very high L_{IR}/L_B value (§ V*d*).

It is noteworthy that these galaxies also have low optical luminosities and therefore may be low-mass systems. Starburst galaxies with similar low levels of far-IR emission are also found in samples of Markarian galaxies (e.g., Weedman 1985; Deutsch and Willner 1987), although they comprise a much smaller fraction of the samples than found here. The smaller number of such systems in the Markarian samples may be due to the fact that relatively few objects with low optical luminosities are included in these samples.

It may be that these systems with high SFRs but low IR emission are relatively low mass systems (compared to typical spiral galaxies) and therefore contain little dust, so that even though the observed color temperature of the dust is moderately enhanced, the total level of IR emission remains quite low. Thus the optical and IR data taken together suggest the existence of a group of objects which are interacting and are experiencing high SFRs, but do not show up strongly in the infrared. This implies that far-IR studies will not automatically pick out all starburst systems.

c) *Disk Star Formation Systems*

We have also compiled a group made up of the relatively few interacting systems that show little evidence of current star-formation activity in their nuclear regions but do show signs of significant activity in their outer disk regions (i.e., the majority of observed Hα emission originates outside of their central regions). Again, these are pairs in which both galaxies exhibit this property. This group of "disk dominated" galaxies has a lower mean L_{IR}/L_B ratio and lower $R(60/100)$ and higher $R(12/25)$ flux ratios than the high (nuclear) SFR galaxies discussed previously (see Table 4). Optical spectra of the star-forming regions in the disks of these galaxies indicate similar stellar population mixes and current SFRs as seen in the active regions of the interacting galaxies with high nuclear-region SFRs. The fact that we see differences in the IR emission properties of galaxies which appear to have similar levels of star formation—the only difference being the location of star-formation activity within the galaxies—many imply differences in the local character of either the actual process of star formation or the environment in which it is taking place. In particular, differences in how densely packed the dust is may be a possibility.

d) *High L_{IR}/L_B Interacting Systems*

As mentioned in § III*a*, there is a group of seven interacting systems that have unusually high L_{IR}/L_B ratios. The mean values of L_{IR}/L_B for this group are 5 and 16 times higher than that of the interacting and isolated galaxy samples, respectively (Table 4). A more detailed look at the properties of these objects reveals the following. First, they all have very high infrared luminosities, ranging from 1.9 to $3.1 \times 10^{11}\ L_\odot$. The mean infrared luminosity of this group of objects is a factor of 4 higher than that of the whole interacting galaxy sample and almost a factor of 20 higher than that of the sample of isolated galaxies. These systems also have $R(60/100)$ and $R(12/25)$ colors that are significantly higher and lower, respectively, than average for the interacting galaxy sample (Table 4). The mean colors for this group are indicated by the label "IR" in Figure 3. The mean $R(60/100)$ color for this group corresponds to a dust temperature of 41 K (assuming emissivity proportional to frequency).

Second, every one of the galaxies in these pairs has a nuclear region (~ 2 kpc) optical spectrum indicative of high levels of current and recent star-formation activity (Bushouse 1986*a*, 1987). The spectrum of the eastern component of the UGC 8335 pair is shown as an example in Figure 8. This spectrum is dominated by very strong H II region-like emission lines with an almost featureless hot-star continuum. Features in the optical spectra of all of the systems in this group are consistent with hot stars being the dominant source of ionization, except for UGC 4509 which has the highest L_{IR}/L_B ratio and exhibits a mild LINER spectrum.

Third, optical images of these systems suggest that three of them—UGC 4509, UGC 8387, and NGC 1614—are merger-type objects, and the remaining systems are either contact pairs or very closely interacting pairs. Finally, four of the seven—NGC 1614, UGC 4509, 6471/2, and 8387—are the only systems in the entire interacting galaxy sample known to exhibit H I 21 cm absorption spectra (Bushouse 1987) and all seven are strong radio sources (Bushouse 1988).

These facts lead us to suggest that very strong interactions, leading to correspondingly high SFRs, are necessary to drive systems to the extreme levels of infrared emission as seen in this group of objects (see also Harwit *et al.* 1987; Joseph and Wright 1985). Conversely, samples of objects selected to contain only extremely infrared-luminous galaxies will almost certainly be biased toward objects of this type (e.g., Elston, Cornell, and Lebofsky 1985; Houck *et al.* 1985; Lonsdale, Persson, and Matthews 1984; Smith *et al.* 1987; Soifer *et al.* 1984).

e) *Ultraluminous IRAS Galaxies*

Sanders *et al.* (1988) have studied various optical and infrared properties of 10 infrared galaxies with luminosities $L(8\text{–}1000\ \mu\text{m}) \geq 10^{12}\ L_\odot$, and find evidence suggesting that nearly all are advanced merger systems with exceptionally luminous nuclei. Optical spectra of these systems indicate a mixture of starbu--t ~nd AGN energy sources. Sanders *et al.* propose that these ultraluminous infrared galaxies represent the initial, dust-shrouded stages of quasars. We have transformed their observational data onto the system used here and present the mean properties of these systems along with our samples of objects in Table 4. The location of the mean infrared colors for these systems is indicated by the letter "U" in Figure 3. As can be seen from the values in Table 4, these systems form an extension to the group of high L_{IR}/L_B interacting pairs in our sample (see previous section). It appears then, that the group of high L_{IR}/L_B systems in our sample may be thought of as being "one step removed" from the extremely active, advanced merger systems in the Sanders sample.

Ultraluminous systems such as these do not appear in our sample of interacting galaxies presumably because they are intrinsically rare (e.g., Soifer *et al.* 1986). Because there are few of them, they will only be found at greater distances. Their greater distance, plus the fact that they are advanced merger systems and hence intrinsically compact, will cause them to have angular sizes and apparent magnitudes below the limit of the UGC, from which the majority of our sample was selected. Furthermore, their small angular sizes would not allow the type of visual scrutiny used in the selection process for our sample of interacting pairs.

f) Other Interacting Samples

Haynes and Herter (1988) have examined *IRAS* data for samples of optically selected isolated and binary galaxies where the binary systems were chosen to have large angular separations (2′–10′) so as to be resolved by *IRAS*. This selection criterion tends to favor relatively nearby close systems or distant systems which have relatively large linear separations. The mean projected separation in this sample is ~ 50 kpc; significantly larger than the mean separation of the interacting pairs studied here, which is ~ 20 kpc. They find that highly luminous infrared emitters are extremely rare in their sample of binary systems and that, on average, the binary galaxies are only marginally more luminous in the infrared than their comparison sample of isolated galaxies.

Kennicutt *et al.* (1987) have studied two samples of interacting galaxies; a "complete" sample of galaxies with close companions, defined independently of any morphological peculiarities, and an intentionally biased sample of unusually disturbed systems drawn from the Arp Atlas. The members of the complete sample are similar to those binary systems studied by Haynes and Herter, but with smaller mean separation and more morphological evidence of tidal perturbations. The Arp sample resembles closely the severely disturbed, close pairs in the interacting sample studied here. They find the median L_{IR}/L_B ratio enhanced by a factor of 1.45 for the complete sample and by a factor of 2.2 for the Arp sample, relative to a comparison sample of isolated galaxies. They also find a population of infrared-bright interacting pairs which is not seen in the control sample.

Joseph and Wright (1985) studied a sample of nine merging galaxies, morphologically selected to appear as a single, coalesced object with tidal tails. They found these merging systems to be extremely luminous infrared sources. Their infrared luminosities are similar to that of the group of high L_{IR}/L_B objects in our sample (§ V*d*), and in fact three of their nine systems are members of our high L_{IR}/L_B group.

The cumulative results of these surveys demonstrate the relationship between the proximity and/or severity of tidal interactions and the resulting activity within the galaxies. There is a steady increase in the average level of star-formation activity (as evidenced by infrared emission) as we examine more closely interacting and more severely disturbed systems. The weakly interacting systems studied by Haynes and Herter show only a marginal increase in infrared luminosity, while the more strongly interacting systems in the Kennicutt *et al.* complete sample show a 50% increase in IR luminosity, and their Arp sample and the sample studied here show about a factor of 2 increase, and finally the merging systems in our high L_{IR}/L_B group and in the Joseph and Wright sample show an increase in L_{IR}/L_B of almost a factor of 16. Telesco, Wolstencroft, and Done (1988) have also found a strong tendency for the *IRAS* $R(60/100)$ color temperature to be the highest for interacting pairs with the smallest separation.

It should be noted, however, that in all cases we are dealing with average values for an entire sample, and that values for individual objects still span a large range. In all of these samples the correlation between pair separation and the level of induced activity exists only in the sense that galaxies with the highest levels of star-formation activity are usually members of close pairs, while galaxies with lower levels of star formation occur at all separations. Thus it appears that many strong starbursts are triggered by close interactions, but close interactions by themselves are not always sufficient to result in a starburst.

VI. CONCLUSIONS

Galaxy-galaxy collisions *can* lead to enhanced infrared emission, but not in all cases. The FIR luminosities of interacting galaxies span a large range, overlapping much of that of isolated disk-type galaxies, but on average interacting galaxies have infrared luminosities that are twice as high as isolated galaxies. Compared to isolated disk galaxies, interacting pairs also have infrared colors indicative of higher than normal interstellar dust temperatures. These facts suggest that the interacting galaxies are experiencing a wide range of star-formation activity and, on average, have higher current SFRs than isolated galaxies. This conclusion is consistent with the results of previous optical studies of the same galaxies. Therefore the IR properties of these galaxies conform, at least in an average way, to the trends suggested by optical studies alone.

High values of infrared excess, $L_{IR}/L_B > 10$, are seen only in interacting systems (and in many of them), suggesting that an interaction is required to induce very high SFRs. This verifies the dominance of interacting systems in previously studied infrared-selected samples. We find as well a group of interacting pairs with extreme values of infrared excess, $L_{IR}/L_B \sim 50$. These pairs are among the most strongly interacting (to the point of merging) members of our sample. This suggests that deeply interpenetrating collisions between galaxies may be a requirement for extreme enhancements in infrared luminosity, as is seen in the sample of ultraluminous *IRAS*-selected systems studied by Sanders *et al.* (1988). Furthermore, there appears to be a luminosity threshold at $L_B \sim 10^9\ L_\odot$, below which galaxies (interacting or isolated) do not experience infrared enhancements.

Infrared excess, as measured by L_{IR}/L_B, and $R(12/25)$ and $R(60/100)$ colors correlate with the optically indicated level of star-formation activity in the interacting galaxies. Infrared excess increases with increasing star-formation activity and the infrared colors imply increasingly warmer $R(60/100)$ temperatures and more thermal emission at 25 μm as the SFR increases.

All galaxies with infrared excesses and higher than normal dust temperatures also have optical indications of high SFRs. Thus we find no case of infrared activity which is not suggested by the optical data. Based on these results, there is no reason to invoke processes other than star formation to account for the enhanced infrared luminosity in these interacting systems.

There are galaxies that have optical indications of high SFRs without infrared excesses. These galaxies may contain little dust and may also be of low mass, suggesting once again that there may be a minimum threshold for enhanced infrared emission. Therefore, it appears that high SFRs are a necessary but not sufficient requirement for enhanced infrared emission in galaxies.

A comparison of the results of this survey with other surveys of different types of paired/interacting galaxies shows a strong tendency for the level of interaction-induced star formation activity to be correlated with the severity of the interaction. Galaxies that are in the process of merging are experiencing the strongest starbursts. Furthermore, while active nuclei seem to be rare in the sample of interacting galaxies studied here, the advanced merger systems of Sanders *et al.* appear to have larger contributions from active galactic nuclei (AGNs). Therefore it is clear that direct collisions, where the galactic disks overlap by a large amount, are required to lead to large enhancements in star-formation activity, and consequently to higher IR luminosities, as well as to the possibility of triggering AGNs.

We wish to thank the staff at IPAC, particularly Carol Lonsdale, for their assistance with the *IRAS* data analysis. This work was supported by NASA through the SADAP/*IRAS* Data Analysis Program. H. B. acknowledges support from the National Research Council.

REFERENCES

Allen, D. A., Roche, P. F., and Norris, R. P. 1985, *M.N.R.A.S.*, **213**, 67P.
Arp, H. C. 1966, *Atlas of Peculiar Galaxies* (Pasadena: California Institute of Technology) and *Ap. J. Suppl.*, **14**, 1.
Bottinelli, L., Gouguenheim, L., and Paturel, G. 1982, *Astr. Ap.*, **47**, 171.
Burstein, D., and Heiles, C. 1982, *A.J.*, **87**, 1165.
———. 1984, *Ap. J. Suppl.*, **54**, 33.
Bushouse, H. A. 1986*a*, *A.J.*, **91**, 255.
———. 1986*b*, Ph.D. thesis, University of Illinois.
———. 1987, *Ap. J.*, **320**, 49.
———. 1988, in preparation.
Catalogued Galaxies and Quasars Observed in the IRAS Survey. 1985, prepared by C. J. Lonsdale, G. Helou, J. C. Good, and W. Rice (Jet Propulsion Laboratory preprint D-1932) (Extragalactic Catalog).
Cutri, R. M., and McAlary, C. W. 1985, *Ap. J.*, **296**, 90.
Dahari, O. 1985, *Ap. J. Suppl.*, **57**, 643.
de Jong, T., *et al.* 1984, *Ap. J.* (*Letters*), **278**, L67.
Deutsch, L. K., and Willner, S. P. 1987, *Ap. J. Suppl.*, **63**, 803.
de Vaucouleurs, G., de Vaucouleurs, A., and Corwin, H. 1976, *Second Reference Catalogue of Bright Galaxies* (Austin: University of Texas Press) (RC2).
Elston, R., Cornell, M. E., and Lebofsky, M. J. 1985, *Ap. J.*, **296**, 106.
Feigelson, E. D., Isobe, T., and Weedman, D. W. 1987, *Ap. J.* (*Letters*), **319**, L51.
Fisher, J. R., and Tully, R. B. 1981, *Ap. J. Suppl.*, **47**, 139.
Gallagher, J. S., Hunter, D. A., and Tutukov, A. 1984, *Ap. J.*, **284**, 544.
Goad, J. W., and Gallagher, J. S. 1985, *Ap. J.*, **297**, 98.
Harwit, M., Houck, J. R., Soifer, B. T., and Palumbo, G. G. C. 1987, *Ap. J.*, **315**, 28.
Helou, G. 1986, *Ap. J.* (*Letters*), **311**, L33.
Houck, J. R., Schneider, D. P., Danielson, G. E., Beichman, C. A., Lonsdale, C. J., Neugebauer, G., and Soifer, B. T. 1985, *Ap. J.* (*Letters*), **290**, L5.
Huchtmeier, W. K. 1982, *Astr. Ap.*, **110**, 121.
Hunter, D. A., and Gallagher, J. S. 1986, *Pub. A.S.P.*, **98**, 5.
Israel, F. 1980, *Astr. Ap.*, **90**, 246.
Joseph, R. D., Meikle, W. P. S., Robertson, N. A., and Wright, G. S. 1984, *M.N.R.A.S.*, **209**, 111.
Joseph, R. D., and Wright, G. S. 1985, *M.N.R.A.S.*, **214**, 87.
Jura, M. 1982, *Ap. J.*, **254**, 70.
Keel, W. C., 1983, *Ap. J. Suppl.*, **52**, 229.
Keel, W. C., Kennicutt, R. C., Hummel, E., and van der Hulst, J. M. 1985, *A.J.*, **90**, 708.
Kennicutt, R. C. 1983, *Ap. J.*, **272**, 54.
Kennicutt, R. C., Keel, W. C., van der Hulst, J. M., Hummel, E., and Roettiger, K. A. 1987, *A.J.*, **93**, 1011.
Kennicutt, R. C., and Kent, S. M. 1983, *A.J.*, **88**, 1094.
Lonsdale, C. J., Persson, S. E., and Matthews, K. 1984, *Ap. J.*, **287**, 95.
Miller, R. H., and Smith, B. F. 1980, *Ap. J.*, **235**, 421.
Nilson, P. 1973, *Uppsala General Catalogue of Galaxies* (Uppsala: Uppsala Offset Center) (UGC).
Persson, C. J., and Helou, G. 1987, *Ap. J.*, **314**, 513.
Rieke, G. H., *et al.* 1985, *Ap. J.*, **290**, 116.
Rieke, G. H., and Lebofsky, M. J. 1985, *Ap. J.*, **304**, 326.
Sandage, A., and Tammann, G. A. 1981, A Revised Shapely-Ames Catalogue of Bright Galaxies (Washington: Carnegie Institution of Washington Publications) (RSA).
Sanders, D. B., Soifer, B. T., Elias, J. H., Madore, B. F., Matthews, K., Neugebauer, G., and Scoville, N. Z. 1988, *Ap. J.*, **325**, 74.
Smith, B. J., Kleinmann, S. G., Huchra, J. P., and Low, F. J. 1987, *Ap. J.*, **318**, 161.
Soifer, B. T., *et al.* 1984, *Ap. J.* (*Letters*), **278**, L71.
Soifer, B. T., Sanders, D. B., Neugebauer, G., Danielson, G. E., Lonsdale, C. J., Madore, B. F., and Persson, S. E. 1986, *Ap. J.* (*Letters*), **303**, L41.
Stauffer, J. R. 1981, Ph.D. thesis, University of California, Berkeley.
Telesco, C. M., Wolstencroft, R. D., and Done, C. 1988, *Ap. J.*, **329**, 174.
Toomre, A., and Toomre, J. 1972, *Ap. J.*, **178**, 623.
Weedman, D. W. 1985, in *Star Formation in Galaxies*, ed. C. Persson (Washington: U.S. Government Printing Office), p. 351.

HOWARD A. BUSHOUSE: Northwestern University, Dearborn Observatory, 2131 Sheridan Road, Evanston, IL 60201

SUSAN A. LAMB: 341 Astronomy Building, 1011 W. Springfield Ave., Urbana, IL 61801

MICHAEL W. WERNER: NASA Ames Research Center, Mailstop 245-6, Moffett Field, CA 94035